Electronic Journal of Biotechnology 74 (2025) 54–72

Contents lists available at ScienceDirect

Electronic Journal of Biotechnology

journal homepage: www.elsevier.com/locate/ejbt

Research article

Exploring the multifaceted bioactivities of silver nanoparticles synthesized from red algae *Hypnea pannosa*: Antimicrobial, antibiofilm, and insecticidal potentials ☆

Mansour A.E. Bashar [a], Enas M.H. Attia [b], Alsayed E. Mekky [c], Tharwat A. Selim [d], Walaa M. Shaban [a], Mohamed A.M. El-Tabakh [a], Ammar.M. Mahmoud [e], Mostafa A. Abdel-Maksoud [f], Ali A. Ali [e], Mohamed A. El-Tayeb [f], Waleed B. Suleiman [c], Mohamed E. El Beeh [g], Sabiha Fatima [h], Bushra Hafeez Kiani [i], Nehal M. Khairy [j,k], Ebrahim Saied [c,*]

[a] *Marine Biology Branch, Zoology Department, Faculty of Science, Al-Azhar University, Nasr City, Cairo, Egypt*
[b] *Physics Department, Faculty of Science (Girls), Al-Azhar University, Nasr City, Cairo, Egypt*
[c] *Botany and Microbiology Department, Faculty of Science, Al-Azhar University, Nasr City, Egypt*
[d] *Zoology and Entomology Department, Faculty of Science, Al-Azhar University, Nasr City, Cairo, Egypt*
[e] *Chemistry Department, Faculty of Science (Boys), Al-Azhar University, Nasr City, Cairo, Egypt*
[f] *Department of Botany and Microbiology, College of Science, King Saud University, Riyadh, Saudi Arabia*
[g] *Zoology Department, Faculty of Science, Mansoura University, Mansoura, Egypt*
[h] *Department of Clinical Laboratory Science, College of Applied Medical Sciences, King Saud University, Riyadh, Saudi Arabia*
[i] *Department of Biology and Biotechnology, Worcester Polytechnic Institute, Worcester, MA, USA*
[j] *Department of Microbiology and Immunology, Egypt Drug Authority, Giza, Egypt*
[k] *Department of Microbiology and Immunology, Faculty of Pharmacy, Sinai University, East Kantara branch, Ismailia, Egypt*

GRAPHICAL ABSTRACT

Exploring the multifaceted bioactivities of silver nanoparticles synthesized from red algae *Hypnea pannosa*: Antimicrobial, antibiofilm, and insecticidal potentials

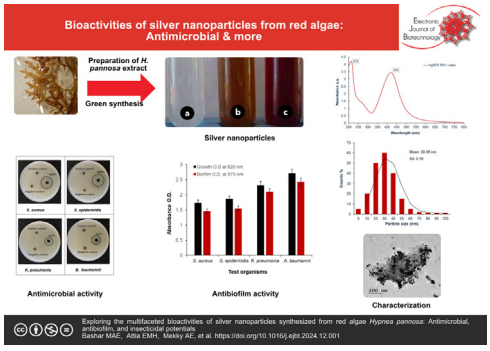

ARTICLE INFO

Article history:
Received 6 September 2024

ABSTRACT

Background: The emergence of microbial resistance to conventional antibiotics and the environmental impact of chemical pesticides necessitates the search for alternative and sustainable solutions. This study

☆ Audio abstract available in Supplementary material.
Peer review under responsibility of Pontificia Universidad Católica de Valparaíso
* Corresponding author.
E-mail address: hema_almassry2000@azhar.edu.eg (E. Saied).

https://doi.org/10.1016/j.ejbt.2024.12.001

Accepted 2 December 2024
Available online 3 February 2025

Keywords:
Adulticidal
Antibiofilm
Antimicrobial
C. pipiens mosquito
Eco-friendly method
Hypnea pannosa
Insecticidal potentials
Larvicidal
Phycosynthesized
Red algae
Silver nanoparticles

explores the utilization of the dried biomass of the red algae *Hypnea pannosa* to synthesize silver nanoparticles (AgNPs) using a green and eco-friendly method.
Results: The synthesized AgNPs displayed sizes ranging from 15 to 60 nm with polydispersed shapes and a face-centered cubic crystalline structure, confirmed through characterization techniques including transmission electron microscopy (TEM), dynamic light scattering (DLS), and X-ray diffraction (XRD). Stability assessments via zeta potential measurements and docking studies of oleic acid and 9,12-octadecadienoic acid against Gyrase B and GST proteins were also conducted. The nanoparticles demonstrated potent antibacterial and antibiofilm activities, particularly against *Staphylococcus epidermidis*. Both the algal extract and the AgNPs exhibited significant larvicidal and adulticidal effects against *Culex pipiens*, with the nanoparticles showing superior efficacy, indicated by lower LC50 and LC90 values. The highest larvicidal effectiveness achieved was 93.33% for algal extract at 600 mg/L and 100% for AgNPs at 100 mg/L.
Conclusions: This study provides a sustainable method for producing AgNPs with diverse applications in medical and mosquito control fields, highlighting their potential as effective and safe alternatives to conventional antibacterial and insecticidal agents.
How to cite: Bashar MA, Attia EM, Mekky AE, et al. Exploring the multifaceted bioactivities of silver nanoparticles synthesized from red algae *Hypnea pannosa*: Antimicrobial, antibiofilm, and insecticidal potentials. Electron J Biotechnol 2025;74. https://doi.org/10.1016/j.ejbt.2024.12.001.

1. Introduction

Antibacterial resistance poses a significant global threat to public health and the economy as it considerably lowers the likelihood of effectively treating infections, thereby increasing the morbidity and mortality associated with bacterial diseases [1]. Between sixty and eighty percent of all bacterial infections in humans stem from bacteria that form biofilms, while the remainder exists in a planktonic state [2]. Microbial biofilms consist of bacterial consortia that colonize surfaces and are embedded within a self-produced matrix, primarily composed of extracellular polymeric substances. These biofilms form irreversible attachments to various surfaces, including living tissues and medical implants such as catheters, valves, and prostheses [3]. Biofilm formation enhances bacterial resistance to harsh environmental factors, such as nutrient fluctuations, changes in oxygen levels, pH, and temperature, as well as to antibacterial agents [4]. Regrettably, increasing the dosage of antibiotics can lead to severe unintended health risks by promoting the spread of multidrug-resistant bacteria, exacerbating public health challenges. Given this context, the pursuit of effective drug compounds has become critically important, as exemplified by research on leprosy treatments [5]. The rise in biofilm resistance to traditional antibiotics underscores the urgency to develop new strategies for treating infections linked to both biofilms and resistant bacteria. In recent times, leveraging nanotechnology has become a primary focus in the innovation of new antibacterial solutions [6].

The unique properties of chemical nanoparticles are in high demand across various industries, both new and established. Traditional chemical methods for synthesizing nanoparticles have seen limited success, leading to a shift towards biological approaches to address several challenges [7]. Consequently, bioreduction methods have gained prominence as an innovative technology for nanoparticle synthesis, addressing the limitations of conventional chemical methods like particle formation, monodispersity, and thermodynamic stability [8]. Moreover, bioreduction through green chemistry processes offers an environmentally friendly and safer alternative to traditional methods [9]. Biological sources such as marine algae have been recognized for catalyzing specific reactions, marking them as practical components of modern biosynthetic strategies [10]. These biological methods provide a greener alternative to non-biological techniques involving ultraviolet radiation, lithography, laser ablation, ultrasonic fields, and photochemical reduction. The use of marine natural products in the synthesis of metallic nanoparticles opens extensive applications in nanotechnology. Biogenic synthesis of nanoparticles is favored over chemical methods, as it does not require the use of energy, high temperatures, high pressure, or toxic chemicals [11]. Marine macroalgae contain a diverse array of chemicals, including flavonoids, alkaloids, steroids, phenols, polysaccharides, saponins, and functional groups such as hydroxyl, carboxyl, and amino. These components act as effective metal-reducing and capping agents, providing a robust single-step coating on metal nanoparticles [12]. The capacity of marine macroalgae to endure severe atmospheric conditions better than other microorganisms is another noteworthy characteristic [13]. Algae are referred to as "bionanofactories" because they use both their dried dead biomass and live biomass in the creation of nanoparticles [14]. Marine algae are widely distributed. It is estimated that there are 1460 million tons of brown and 261 million tons of red seaweed resources worldwide. The total yearly output of seaweed is projected to be 17.21 million tons of wet weight [15]. The genus *Hypnea*, belonging to the family *Cystocloniaceae* and order Gigartinales, is prevalent in warm and temperate seas. Species such as *Hypnea musciformis*, *Hypnea pannosa*, and *Hypnea valentiae* are notable sources of both agar and carrageenan, valuable hydrocolloids used in various industries [16]. Historically, silver (Ag) has been employed in various applications such as wound healing using silver plates, treating ulcers, and as a 1% $AgNO_3$ solution for neonatal eye infections [17]. While silver is an excellent conductor of electricity, its high cost limits its usage in the electrical industry. Nevertheless, $AgNO_3$ play a significant and highly effective role due to their unique thermal, optical, electrical, and biocidal properties [18].

Due to their potent biocidal activity, silver nanoparticles are increasingly used in the medical field to target pathogenic microbes that have developed resistance to multiple antibiotics, which has become a significant and growing public health concern. It is crucial, therefore, to develop new techniques to control pathogenic microbes [19]. $AgNO_3$ can inhibit bacterial growth by interacting with the bacterial cell wall, disrupting it, and thereby hindering protein synthesis, leading to cell death [20]. $AgNO_3$ synthesized by algae are particularly effective due to their hydrophilic surface groups such as sulfate, carboxyl, and hydroxyl, enhancing their medical applicability. Algae are advantageous as they do not produce any toxic or harmful substances during this process [21]. The bio-reduction of metal ions to nanoparticles takes place

extracellularly on the algal cell surface, while intracellularly, it occurs through enzymatic activity within the cell wall and membrane [22].

The significance that mosquitoes play in the spread of illness makes them a serious worldwide health problem. Around 51 million cases of lymphatic filariasis are thought to have been caused by the *Culex* species, which is particularly common in urban and semi-urban areas of Africa and Asia [23]. In Egypt, *Culex pipiens* is widespread and transmits several pathogens including the Rift Valley fever virus, *Washeteria bancroftian*, and the West Nile virus [24]. Recent studies have also explored the potential for transmitting the hepatitis C virus via mosquitoes [25].

Controlling mosquitoes is crucial to curtail the spread of these diseases and protect public health. Traditional mosquito control strategies predominantly involve synthetic insecticides like organochlorines and organophosphates, but these have often fallen short due to human, environmental, and economic concerns [26]. Consequently, there is a growing interest in natural alternatives, including plant and marine products [23,27,28], for more sustainable insect control. The synthesis of nanoparticles from natural sources presents a promising approach due to its eco-friendly advantages, safety, and cost-effectiveness [29].

The multifunctional properties of AgNPs made using *H. pannosa* extracts are investigated in this work. These biosynthesized AgNPs' physicochemical characteristics were examined utilizing a variety of methods, such as zeta potential tests, UV–vis spectroscopy, XRD, TEM, DLS, and FTIR. The biological activities of the AgNPs were also investigated in this work, with an emphasis on their antibacterial activity against both Gram-positive and Gram-negative. Additionally, these biosynthesized AgNPs were evaluated for their larvicidal and adulticidal properties against the *C. pipiens* mosquito, indicating their potential for use in public health applications.

2. Materials and methods

2.1. Chemicals

Hi Media, a company based in Cairo, Egypt, provided all the scientific-grade chemicals and reagents utilized in the current investigation. Every experimental technique was conducted using freshly made double-distilled water.

2.2. Collection of red alga

H. pannosa, the red alga, was collected in the Red Sea from a depth of 1 to 10 m in Dahab city, which is situated in the Gulf of Aqaba. The algal samples were collected and then brought in plastic bags to the lab. The samples were thoroughly cleaned in the lab using running tap water to get rid of epiphytes, sea salt, and other impurities. After allowing the alga to dry naturally at room temperature, they were blended into a powder using an electric blender.

2.2.1. Preparation of the red alga extract

With minor adjustments, the preparation technique was modified from an earlier documented process [30]. Two grams of the powdered algae were weighed and added to one hundred milliliters of deionized water for the extraction procedure. After that, this combination was heated for 30 min at 80°C in a water bath. The extracts were boiled and then allowed to cool to ambient temperature before being filtered using Whatman filter paper. These extracts were kept for future use at 4°C because they include substances that function as both stabilizing and reducing agents.

2.2.2. Ecofriendly synthesis of AgNP

A 45 mL solution containing 1 mM of silver nitrate was made. Five milliliters of the algal extract were added to this mixture gradually while it was left at room temperature and constantly stirred. The solution's hue first became a faint pink throughout this phase. The hue intensified to dark brown after a further 24–48 h of incubation, signifying the creation of AgNP [30].

2.3. Characterization

2.3.1. UV–visible spectroscopy

The UV–visible spectroscopy spectrum was recorded using a JASCO V-630 spectrometer. The sample was diluted in deionized water, and the absorbance was measured over a wavelength range of 200–800 nm using quartz cuvettes with a 1 cm optical path. Deionized water filled in a quartz cuvette served as the reference. The scanning speed was set at 500 nm/min.

2.3.2. Fourier transform infrared spectroscopy

The biomolecules in the algal extract that are reducing Ag ions and capping the ensuing AgNPs were found using FTIR. An Agilent system Cary 660 FT-IR model was used for the analysis, which covered a 400–4000 cm^{-1} spectrum range.

2.3.3. X-ray diffraction

A Philips X'Pert Pro X-ray diffractometer located in Eindhoven, the Netherlands, was used to evaluate the crystallinity of the biosynthesized AgNPs. The investigation was conducted across a 2θ range of 4–80° at 40 kV of voltage and 30 mA of current. The Debye-Scherrer equation [31] was utilized to compute the mean size of the nanoparticle.

$$D = (K\lambda/\beta \cos\theta) \quad [32]$$

Where D is the mean particle size, K is the Scherrer's constant and is equal to 0.9, λ is X-ray wavelength, β is the half of the maximum intensity, and θ is the Bragg's angle.

2.3.4. Transmission electron microscopy and dynamic light scattering

TEM analysis was conducted with a JEOL 1010 microscope operated at 200 kV. A drop of the nanoparticle solution was placed on a carbon-coated copper grid to dry before examination. DLS measurements were performed to assess the size distribution and homogeneity of the biosynthesized AgNPs in colloidal solutions. The analysis was done using a Zetasizer Nano ZN, Malvern Analytical Ltd., Malvern, UK, at a constant temperature of 25°C and a scattering angle of 173°. DLS analysis also provided the polydispersity index (PDI) of the solutions [33].

2.3.5. Zeta potential

The stability and cohesion of the colloidal nanoparticles were investigated via zeta potential analysis using a Zetasizer Nano-series (Nano ZS), Malvern, UK. The nanoparticles were resuspended in distilled water for this measurement, providing insights into the colloidal stability through the magnitude of the zeta potential [34].

3. GC–MS assay

The components of the algal extract were analyzed, quantified, and identified using gas chromatography-mass spectrometry (GC–MS). By comparing the spectra of the detected compounds with those in the NIST 11 and WILEY 09 (Wiley, New York, NY, USA) databases, the compounds' properties were ascertained. These components' molecular weights and chemical characteristics were also recorded, giving rise to a comprehensive compositional profile of the extract [35].

4. Molecular docking

The Gaussian 09 software's output was used to construct the material structures in PDB file format. Gyrase B (PDB ID: **4uro**) and GST (PDB ID: **1PN9**) crystal structures were obtained from the protein data bank (https://www.rcsb.org). The MOE 2015 program was used to carry out molecular docking investigations.

5. Antimicrobial activity

5.1. Test organisms

Four strains of bacterial human pathogens were isolated: *Acinetobacter baumannii*, *Klebsiella pneumoniae*, *Staphylococcus aureus*, and *Staphylococcus epidermidis*. These infections were identified mainly by biochemical analysis, morphological inspection, and culture, all in accordance with the guidelines provided in Bergey's Manual of Determinative Bacteriology [36].

5.1.1. In vitro antimicrobial activity

Using the agar well diffusion method, an in vitro antibacterial study was performed against four harmful bacteria: *S. aureus, S. epidermidis, K. pneumoniae*, and *A. baumannii*. The pathogens were cultured in nutrient broth. Overnight cultures were produced for the experiments to reach a 1.5×10^6 CFU/mL cell density. Mueller-Hinton agar [37] was sterilized and then added to petri plates and let dry.

Using sterile cotton swabs, new cultures of the four pathogens that had grown overnight were applied to the solidified agar. Next, a sterile borer was used to make wells in the agar. In each well, 100 μL of 4000 μg/mL of AgNPs were added, and distilled water was added to the control well [38]. As an additional positive control, a conventional antibiotic disc (cefuroxime) was manually put on the petri plate. Overnight, the plates were incubated at 37°C. The next day, inhibition zones surrounding the wells were observed to determine whether the therapy was successful [39].

5.1.2. Preparation of resazurin solution

Using a vortex mixer, 0.002 g of resazurin salt powder was dissolved in 10 mL of distilled water to prepare the solution. The resulting mixture was filtered through a 0.2 μm Millipore membrane filter to ensure sterility and remove any particulate matter. The filtered solution was then stored at 4°C for 15 d to maintain its stability, as described by Mekky et al. [40].

5.1.3. Determination of minimum inhibitory concentration (MIC) for bacteria

The procedure described in the guideline [41] was used to calculate the MIC. The experiment was carried out using the conventional broth microbiological dilution method in a 96-well round bottom microtiter plate. A 1.5×10^6 CFU/mL inoculum concentration was used.

In order to conduct the microtiter plate MIC test, 100 μL 1000 μg/mL of the AgNPs stock solution was first added to the fourth column. Next, the bacterial inoculum was serially diluted twice in 100 μL of Mueller Hinton Broth (MHB), which was added from the fourth to the twelfth column. AgNP concentrations ranged from the greatest in the fourth column to the lowest in the twelfth column. With both cultures and mediums present, the first column functioned as a positive control, and the second column, which contained just medium, acted as a negative control [42]. After that, 30 μL of resazurin solution was added to each well of the microplate, and it was incubated for 24 h at 37°C. The color change in the wells was used to observe the findings; a blue or purple hue indicated no bacterial development, whereas a pink or colorless tint showed bacterial growth. The AgNPs' colorimetric shift makes it simple to determine the degree of bacterial suppression.

5.1.4. Determination of minimum bactericidal concentrations (MBCs)

Using a macro broth dilution experiment, as previously described in the CRyPTIC Consortium [41], different modifications were made to assess the MBCs of AgNPs against the tested pathogenic isolates. AgNPs were present in the medium used to develop cultures. To find the MBCs, two-fold dilutions of AgNPs at different concentrations (from 1000 to 2.0 μg/mL) were made for the treatment. The overnight-grown cultures from every concentration were streaked onto agar plates after treatment. Finding the MBCs (the lowest concentration of AgNPs at which no bacterial growth is seen on the agar plates, indicating that all the bacteria were killed) was a critical stage in the process.

6. Determination of biofilm formation

6.1. Microtiter plate method

After being cultured for 18–24 h, the bacterial isolates were added to 0.5 McFarland standard suspensions. AgNPs were generated in a range of concentrations, from 32 μg/mL to 1 μg/mL, with a control group containing 0 μg/mL. Using tryptic soy broth (TSB), the bacterial cell concentrations were adjusted to 1.5×10^5 CFU/mL. Following the inoculation, 200 μL aliquots containing the bacterial suspension were placed onto transparent plastic cell culture plates with covers that had a flat bottom. The plates were then incubated aerobically for 24 h at 37°C. All that was in the negative control wells was TSB. Each plate's optical density (OD) at 620 nm was measured following incubation. Except for the negative controls, all wells had OD values greater than 1. After discarding the liquid contents of the wells, 250 μL of sterile phosphate-buffered saline was used to wash each well three times. A total of 200 μl of 99% methanol was then used to fix the remaining clinging microorganisms.

150 μL of 1% crystal violet was used to stain the fixed bacteria, and it was left at room temperature for 15 min. Excess pigment was removed from the surface using running tap water after coloring. The pigmented biofilms were resolubilized in 160 μL of 33% (v/v) glacial acetic acid after the plates were allowed to dry air. To determine the degree of biofilm development, the OD of the resolubilized biofilm solution was measured at 570 nm using a micro-ELISA automated plate reader (Spectra max 250 Microplate Reader, Molecular Devices, Sunnyvale, CA, USA). To guarantee the accuracy and consistency of the findings, each experimental setup was carried out three times [43].

7. Larvicidal activity

In accordance with the World Health Organization methodology [44], the larvicidal activity of the crude algal extract and the biosynthesized silver nanoparticles was assessed against the *C. pipiens* mosquito. Ten early third-instar mosquito larvae were collected and put into 250 mL plastic cups with 125 mL of tap water (124 mL of water and 1 mL of the tested concentration). To compare the results with those of other nano-size extracts at concentrations of 200, 300, 400, 500, and 600 mg/L, algal extract was evaluated. AgNPs that had been synthesized were added in increments of 20, 40, 60, 80, and 100 mg/L. Three duplicates of each concentration were tested. Tests were conducted on the control group using the same settings (10 larvae in 125 mL tap water) for both extracts. The percentage of deaths was noted 24 h after therapy.

7.1. Adulticidal activity

The World Health Organization's bioassay tube method was used to determine adulticidal activity [23]. Ten female mosquitoes were taken from the colony and placed into a plastic tube (holding portion) for one hour. After that, they were carefully moved to the other side (exposure portion), which had Whatman filter paper No. 1 (10 × 10 cm), which were coated with both crude and biosynthesized silver nanoparticles. Papers treated with distilled water and silver nitrate were presented to the control group. In terms of larvicidal activity, the adult was subjected to the same range of concentrations (in both algal extract and AgNPs). Following the exposure period, the mosquitoes were carefully placed back onto the holding section, where they had been for the previous 24 h, and given a cotton ball soaked in a 10% sucrose solution to place on top of the mesh net. Three duplicate tests were conducted on each concentration. Adult mortality was noted 24 h after exposure, and Finney's [45] approach of employing probit analysis to determine the fatal amounts (LC50 and LC90) was used.

8. Statistical analysis

For every treatment, descriptive statistics such as mean and standard deviation (SD) were computed. Probit analysis was used to get the chi-square value, LC50, and LC90 at 95% confidence intervals based on the mean larval mortality data. Using SPSS (Ver. 25), one-way analysis of variance, lower and upper confidence limits, and chi-square values were performed. Pairwise comparisons were performed using the LSD posthoc test. Treatments with silver nitrate showed little larval mortality.

9. Results

9.1. Synthesis and characterization of AgNPs

The formation of AgNPs in the solution was indicated by a dark brown color change, with the appearance of a plasmon resonance peak at 420 nm (Fig. 1). The SPR band is established by the excitation of free electrons, which is responsible for this broad peak in the visible spectrum. This excitation is made easier in metallic nanoparticles such as AgNPs by the closeness of the valence and conduction bands. The bioactive substances in *H. pannosa* mediate the reduction process of the Ag^+ ions into Ag^0 nanoparticles. In the manufacture of AgNPs, these chemicals serve as both stabilizing and reducing agents. The transformation typically occurs within a 24- to 48-h period, showcasing the effective role of *H. pannosa* extracts in facilitating the nanoparticle synthesis.

9.2. FT-IR

The FT-IR study conducted on the red algae extract provided detailed insights into the biomolecules responsible for the reduction of Ag^+ ions to Ag^0, as depicted in Fig. 2. The analysis identified several distinct bands, each corresponding to different functional groups within the algal's biochemical composition, crucial for the bioreduction process. Based on the analysis, the following bands were identified: C—H, C═C, and C—O; C—C stretching, C—O—C and C—O—H deformation vibrations of polysaccharides; CH_2, enol, and amide groups; carboxyl groups; and the bands at 3222, 2925, 2355, 1570, 1504, 1386, 1044, 830, 674, 616, and 464 cm^{-1}.

9.3. X-ray diffraction analysis

XRD analysis confirmed the synthesis of AgNPs and crystalline structure was formed at 10°–60° theta ranges (Fig. 3). The XRD patterns obtained were observed at values, 27.27°, 31.98°, 38.03° and 44.20 in correspondence to height values of 38.61, 21.36, 210.58 and 46.33, respectively (Table 1). AgNP formation was verified at 38.03° and 44.20° in the 2-theta range. AgNPs produced by *H. pannosa* exhibit a crystalline structure and cubic phase, as shown by their XRD pattern. At 2 Theta (38.03°), the crystalline peak was reached with a size of 76.4 and an intensity of 100%. The crystalline structures of AgNPs were confirmed by the sharpness of all obtained peaks.

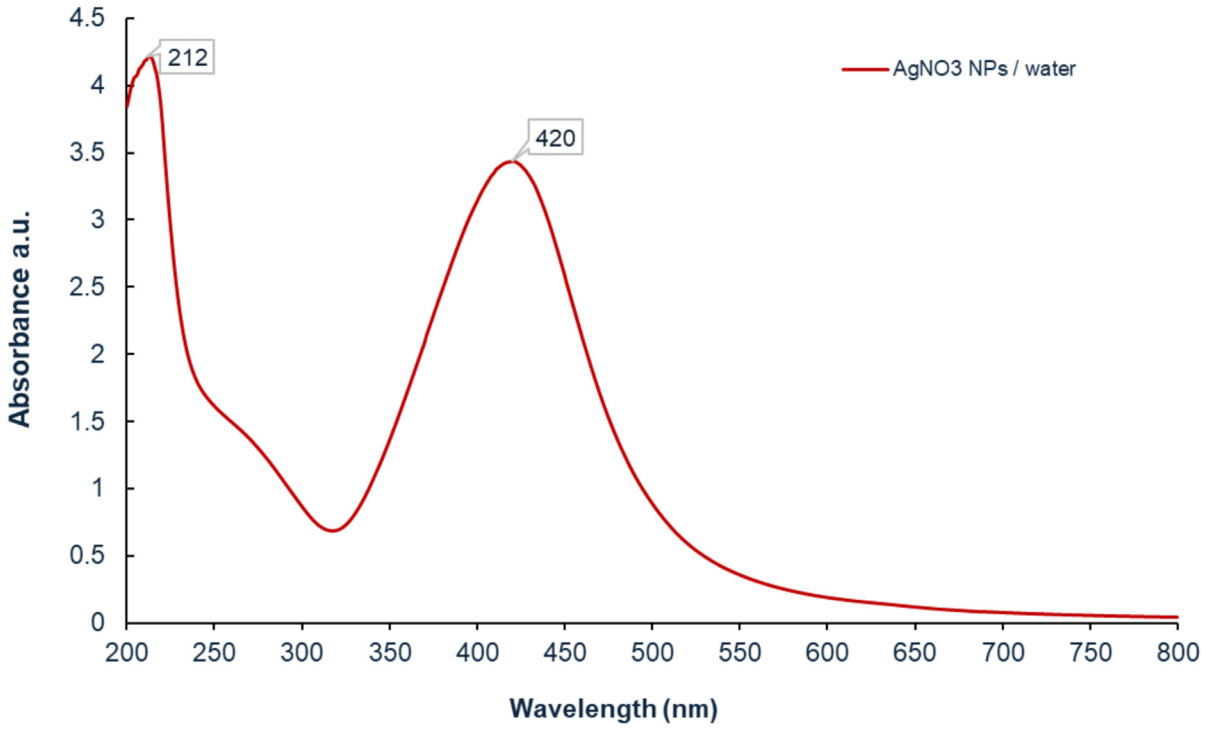

Fig. 1. UV–visible spectrum of AgNPs synthesized from *H. pannosa* extract.

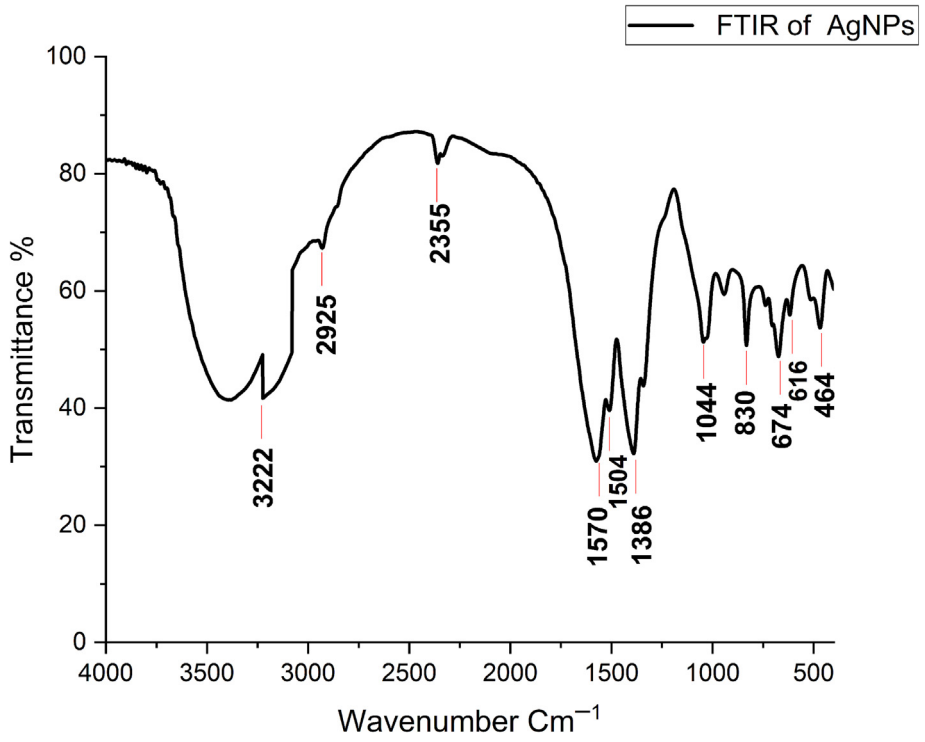

Fig. 2. FT-IR spectrum of biosynthesized AgNPs.

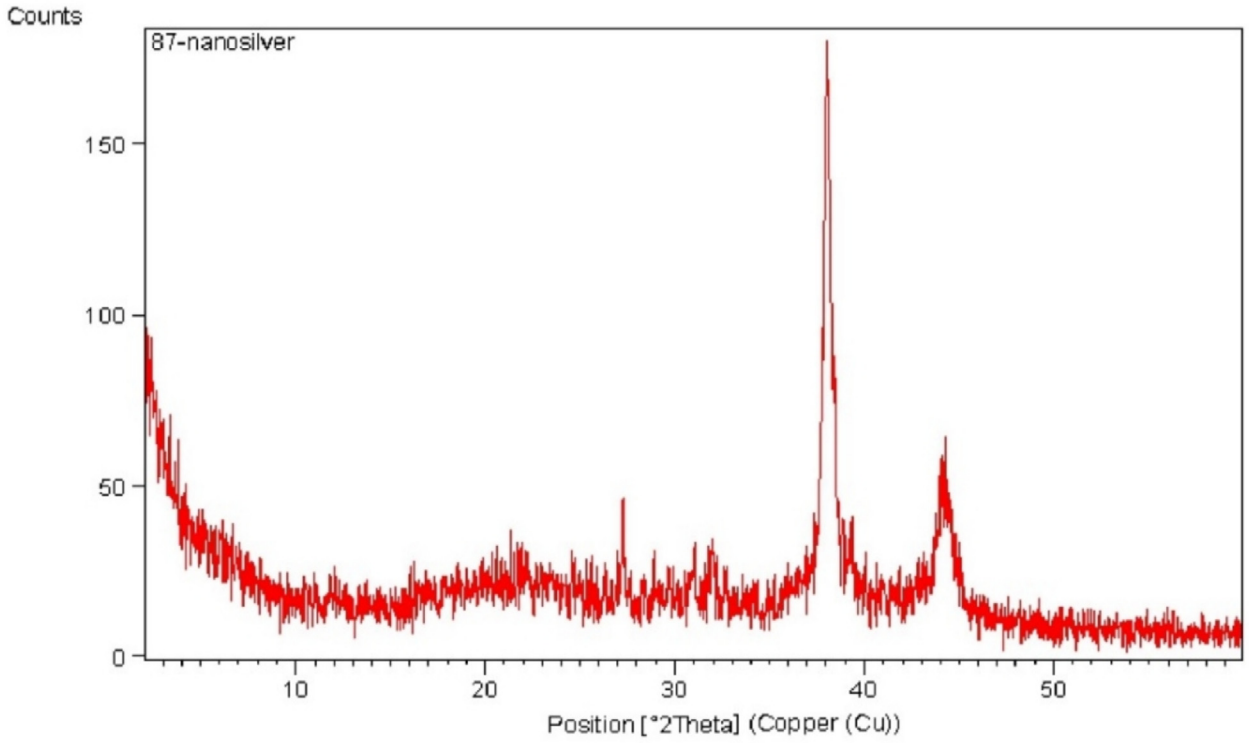

Fig. 3. XRD profile for AgNPs synthesized using *H. pannosa.*

9.4. TEM

Fig. 4a presents a TEM image of AgNPs synthesized using *H. pannosa*. The TEM analysis reveals that the nanoparticles are polydispersed, including hexagons and their sizes range from 15 to 60 nm. This size estimation was determined by measuring the diameters of over 55 particles from the TEM images. Fig. 4b displays histograms corresponding to the data from Fig. 5a, illustrating the size distribution. Results showed an average particle size of 30.56 ± 0.39 nm. The smaller size of these particles enhances their

Table 1
Peaks list of XRD analysis for AgNPs.

Peak Number	Pos. [°2Th.]	d-spacing[nm]	Height [cps]	Rel. Int. [%]
1	27.2727	3.27002	38.61	18.34
2	31.9863	2.79809	21.36	10.14
3	38.0315	2.36609	210.58	100.00
4	44.2064	2.04886	46.33	22.00

surface area, potentially increasing their catalytic effectiveness. Additionally, the crystalline quality of the phyco-synthesized AgNPs is confirmed by the Selected area electron diffraction (SEAD) [46] pattern shown in Fig. 4c, which exhibits distinct circular rings due to Bragg's reflections at 27.27, 31.98, 38.03, and 44.20, indicating the crystalline structure of the nanoparticles.

9.5. Particle size and zeta potential

Using a particle size analyzer in an aqueous environment, the surface charge properties and particle size distributions of the biosynthesized AgNPs were assessed. The size of the refined nanoparticles was measured using a Malvern instrument after they were suspended in double-distilled water with a neutral pH. Fig. 5 presents the results, which show that the AgNPs have a surface charge of −43.4 ± 10.6 mV, as shown by their zeta potential. This suggests that the nanoparticles possess a stable dispersion due to their surface charge. The particle size distribution is detailed in Fig. 6a, which confirms an average particle size of 38.58 nm. This size closely matches the results obtained from TEM analysis, underscoring the consistency of the measurement techniques. The particles are also polydisperse in size, with the larger particles being greater than 80 nm Fig. 6b. Additionally, the PDI was recorded at 0.848, indicating a broad range of particle sizes within

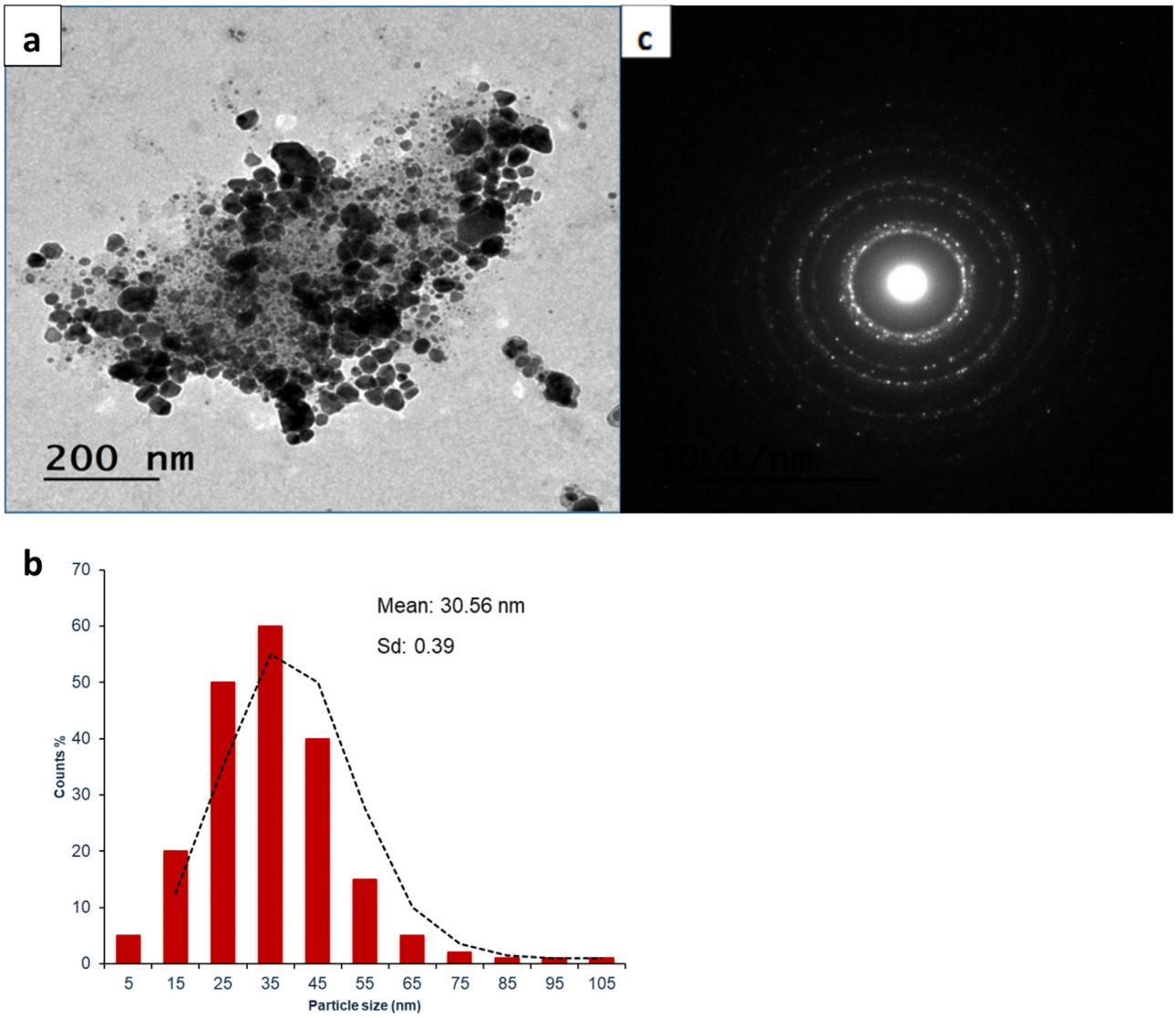

Fig. 4. Characterization of AgNPs synthesized from *H. pannosa* extract. (a) Representative TEM image of AgNPs, illustrating their morphology. (b) Histogram showing the particle size distribution, indicating a range of sizes with an average diameter. (c) SAED pattern confirming the formation of spherical nanoparticles, demonstrating their crystalline nature.

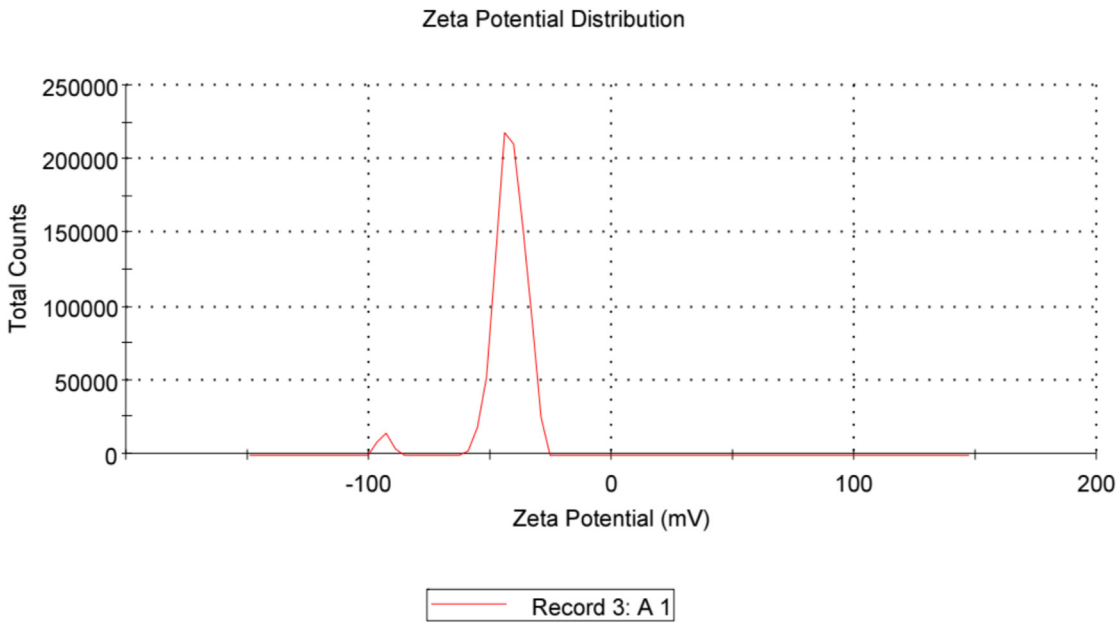

Fig. 5. Zeta potential distribution of synthesized AgNPs.

the nanoparticle preparation. This variance suggests that while the nanoparticles are predominantly uniform, there exists a distribution of smaller and larger particles within the sample.

9.6. GC–MS analysis

Table 2 displays the results from the GC–MS analysis, showing that more than 90% of the compounds identified in the *H. pannosa* extract correspond to entries in the NCBI database. The major constituents identified in the extract include Oleic Acid, which is the most abundant at 24.5%, followed by 9,12-Octadecadienoic acid at 15.16%, its ethyl ester form at 10.2%, and Lupeol at 7.5%. Additionally, several other compounds were detected in smaller quantities: n-Hexadecenoic acid at 6.22%, R-1 Methanandamide at 1.6%, Glycidyl oleate at 1.5%, Trilinolein at 0.84%, 10-Octadecenoic acid, methyl ester at 0.79%, and 14-Methyl pentadecanoic acid, methyl ester at 0.67%. These results outline the diverse chemical composition of the *H. pannosa* extract, highlighting the presence of various fatty acids and other bioactive compounds in significant proportions.

9.7. Docking investigation

Docking on Gyrase B's receptor (PDB ID: **4uro**): Re-docking the co-crystallized Novobiocin (Ligand) in the enzyme binding pocket with an energy score (S) = –5.5125 kcal/mol served as the first validation of the docking process. Oleic acid and 9,12-octadecadienoic acid with the Gyrase B protein (PDB ID: 4uro) receptor were discovered to have docking energy scores of –6.5932 and –6.5557 kcal/mol, respectively, which are greater than the co-crystallized ligand as indicated in Table 3. The greater the engagement, the lower the energy score. As a result, the interaction occurred in the following order: Oleic Acid> 9,12-Octadecadienoic acid> Novobiocin (Ligand). These findings are consistent with the experimental findings of *in-vivo* assay of anti-bacterial activity (Fig. 7).

Docking with the GST receptor (PDB ID: **1PN9**): An energy score (S) of –5.5076 kcal/mol was obtained by redocking the co-crystallized s-Hexylglutathione ligand (GTX) into the enzyme's binding pocket to validate the docking process. The docked oleic acid and 9,12-octadecadienoic acid with the GyraseB protein (PDB ID: **4uro**) receptor were then found to have higher docking energy scores than the co-crystallized ligand, as shown in Table 4. These scores were –5.9952 and –6.0975 kcal/mol, respectively. It is worth noting that a lower energy score corresponds to a greater level of engagement between the ligand and receptor. Accordingly, the interaction was observed to occur in the following order: 9,12-Octadecadienoic acid > Oleic Acid > Novobiocin (Ligand). These outcomes are in line with the experimental results obtained from the in-vivo assay of anti-pesticide activity of the extract (Fig. 8). Comparing experimental data to data generated by theoretical calculations reveals that the two types of data are comparatively comparable. It is acknowledged that the most important factor affecting a compound's biological activity against proteins is interaction.

9.8. Antibacterial activity

The antibacterial efficacy of AgNPs synthesized using *H. pannosa* extract has been clearly demonstrated in our research. We assessed the antibacterial activity of these AgNPs against four pathogenic bacteria known to cause serious diseases. The assessment was conducted using the agar well diffusion method, where the formation of an inhibitory zone around the wells containing the nanoparticles indicates effective antibacterial activity. Our findings revealed that the AgNPs exhibited substantial zones of inhibition, which varied among the tested pathogens. The largest zone of inhibition was 32 mm against *S. epidermidis*, followed by 21 mm against both *S. aureus* and *A. baumannii*, and 16 mm against *K. pneumoniae*, as detailed in Fig. 9 and Table 5. The control tests, both negative (no treatment) and positive (standard antibiotic), did not show clear zones of inhibition, underscoring that the antimicrobial activity observed was solely attributable to the tested nanoparticles. This result highlights the potential of AgNPs as an effective antibacterial agent against multiple harmful bacterial strains.

The MIC refers to the lowest concentration of nanoparticles that effectively inhibits microbial growth. In this study, the MIC for AgNPs synthesized from *H. pannosa* extract was determined using the MTT assay, conducted on a 96-well microtiter plate, with

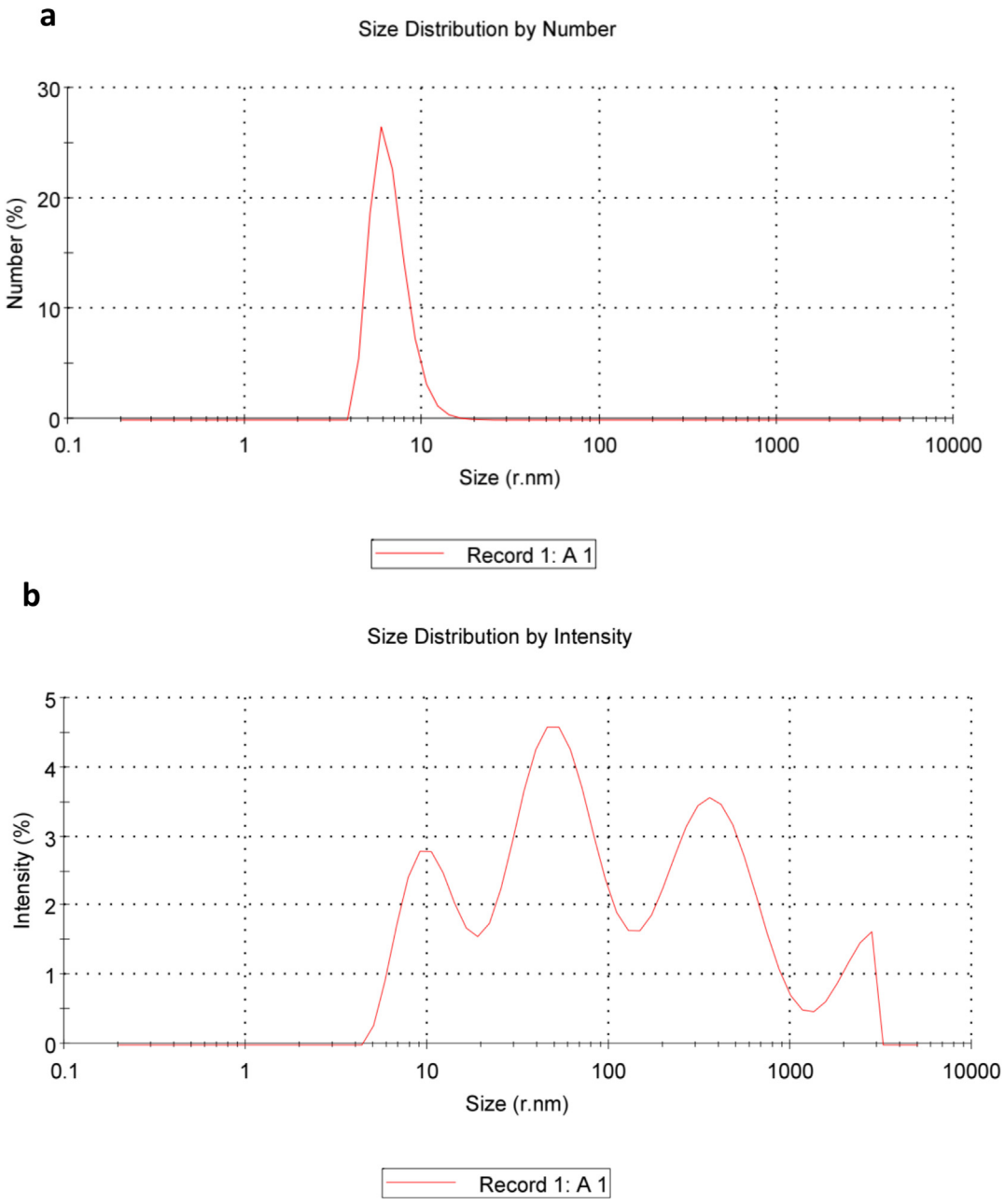

Fig. 6. A, b. Size distribution analysis of biosynthesized AgNPs as measured using DLS particle size analyzer.

results assessed through visual analysis. For each tested bacterial species, growth inhibition was achieved at their respective MIC values. The MIC values for the AgNPs were observed across a range from 1000 to 2.0 μg/mL against pathogens such as *S. epidermidis, S. aureus, K. pneumoniae*, and *A. baumannii*. The data in Table 6 illustrate that the AgNPs significantly enhance bactericidal activity. Specifically, the MIC for *K. pneumoniae* was noted at a higher concentration (32.0 μg/mL), indicating that this pathogen requires a greater number of nanoparticles for effective inhibition. In contrast, the growth inhibitory activity for the other bacterial strains was observed at a lower concentration, specifically 16.0 μg/mL (Fig. 9). Furthermore, the MBC was determined as the lowest concentration at which no visible growth of the test bacteria was observed, recorded at 32 μg/mL for all tested strains.

9.9. Antibiofilm activity of AgNPs

AgNPs synthesized from *H. pannosa* extract were assessed for their anti-biofilm activity in a dose-dependent study targeting biofilm-forming bacteria. The in vitro experiments were designed to evaluate how well these nanoparticles inhibit the formation of biofilms by bacterial species such as *S. epidermidis, S. aureus, K. pneumoniae*, and *A. baumannii*. The results, depicted in (Fig. 10), indicated that the AgNPs effectively prevented biofilm development across the range of tested concentrations. The data demonstrated that the anti-biofilm activity of the AgNPs was most potent against *A. baumannii*, with an effectiveness value of 2.710. This was followed by *K. pneumoniae*, which had a value of 2.320, *S. epidermidis* with 1.870, and *S. aureus* with 1.740. These values

Table 2
GC Mass identification of *H. pannosa* extract.

No.	RT	Compounds	Molecular formula	Molecular weight	Peak area (%)
1	29.42	Oleic Acid	$C_{18}H_{34}O_2$	282	24.56
2	29.22	9,12-Octadecadienoic acid	$C_{18}H_{32}O_2$	280	15.16
3	37.73	9-Octadecenoic acid (Z)-, 2-hydroxy-1-(hydroxymethyl)ethyl ester	$C_{21}H_{40}O_4$	356	10.23
4	29.79	LUP-20(29)-ENE-3,28-DIOL, (3á)-	$C_{30}H_{50}O_2$	442	9.13
5	29.86	Lupeol	$C_{30}H_{50}O$	426	7.54
6	26.2	n-Hexadecenoic acid	$C_{16}H_{32}O_2$	256	6.22
7	30.16	Lupeol	$C_{30}H_{50}O$	426	5.31
8	37.61	9,12-Octadecadienoic acid (Z,Z) –, 2-hydroxy-1-(hydroxymethyl)ethyl Ester	$C_{21}H_{38}O_4$	354	3.34
9	28.96	Lupeol	$C_{30}H_{50}O$	426	2.43
10	28.53	Lupeol	$C_{30}H_{50}O$	426	2.13
11	45.01	R-1 Methanandamide	$C_{23}H_{39}NO_2$	361	1.63
12	34.71	Glycidyl oleate	$C_{21}H_{38}O_3$	338	1.52
13	35.09	Hexadecanoic acid, 2-hydroxy-1-(hydroxymethyl)ethyl ester	$C_{19}H_{38}O_4$	330	0.91
14	42.47	Trilinolein	$C_{57}H_{98}O_6$	878	0.84
15	28.71	10-Octadecenoic acid, methyl ester	$C_{19}H_{36}O_2$	296	0.79
16	41.59	FLAVONE 4′-OH,5-OH,7-DI-O-glucoside	$C_{27}H_{30}O_{15}$	594	0.74
17	34.57	9,12-Octadecadienoic acid (Z,Z)-, 2-hydroxy-1-(hydroxymethyl)ethyl ester	$C_{21}H_{38}O_4$	354	0.71
18	25.54	Pentadecanoic Acid, 14-Methyl-, Methyl Ester	$C_{17}H_{34}O_2$	270	0.67
19	33.8	9-Octadecenoic Acid (Z)-, 2-Hydroxy-1-(Hydroxymethyl) Ethyl Ester	$C_{21}H_{40}O_4$	356	0.63
20	30.71	9,12,15-Octadecatrienoic acid, 2,3-dihydroxypropyl ester, (Z,Z,Z)-	$C_{21}H_{36}O_4$	352	0.61

Table 3
Docking interaction data computations between the active site of the Gyrase B protein receptor (PDB ID: **4uro**) and Novobiocin (Ligand) in the enzyme binding pocket, as well as oleic acid and 9,12-octadecadienoic acid.

Compound	Energy score (S) (Kcal/mol)	Affinity Bond strength (Kcal/mol)	Affinity Bond length (in A° from main residue)	Amino acids	Ligand	Interaction
Novobiocin (Ligand)	–5.5125	–0.9	3.81	ILE 86	6-ring	pi-H
		–0.6	4.72	ARG 144	6-ring	pi-cation
Oleic acid	–6.5932	–2.2	2.8	ILE 51	O 53	H-donor
9,12-Octadecadienoic acid	–6.557	–2.3	2.69	VAL 79	O 51	H-donor

suggest a relative measure of the nanoparticles' efficacy in preventing biofilm formation, with higher values indicating stronger inhibition. This study underscores the potential of AgNPs as effective anti-biofilm agents, offering promising applications in preventing bacterial colonization and biofilm formation on various surfaces, which is crucial for managing infections, especially in medical settings.

9.10. Larvicidal and adulticidal properties against vector C. pipiens mosquito

Five concentrations of manufactured AgNPs (20, 40, 60, 80, and 100 ppm) and the algal extract (200, 300, 400, 500, and 600 mg/L) were applied to the third instar larvae of the tested *C. pipiens* mosquito. The recorded LC50 and LC90 values for the algal extract were (349.786 and 620.378 mg/L), whereas the AgNPs were (43.674 and 88.377 mg/L), according to the data shown in Table 7. No larval mortality was seen in the group treated with $AgNO_3$ solution (without algal extract), and the highest larvicidal activity of both crude algal and synthesized AgNPs (93.33 and 100%) was attained at doses of 600 and 100 mg/L compared with the control group. In the same context, the same concentration treated before with larvae showed high adulticidal activity against adult and it became crystal clear when recorded LC50 and LC90 values of both algal and synthesized AgNPs were (299.810 and 543.004 mg/L) and (45.595 and 102.121 mg/L), respectively. Adult mortality reached 96.67% at 600 mg/L of algal extract while reached the same concentration (96.67%) at 100 mg/L of AgNP extract (Table 8). Generally, *C. pipiens* adults were found to be more susceptible to the synthesized AgNP extract than the algal extract.

10. Discussion

10.1. Synthesis and characterization of AgNPs synthesized by H. pannosa

The production of AgNPs was visually confirmed through a change to a dark brown color. UV–visible spectroscopy showed that the SPR band for AgNPs appeared at 420 nm. Abdel-Raouf et al. [46] noted that *Galaxaura elongata* extracts turned to an intense brown after 3 h of exposure to $AgNO_3$. Similarly, Dhas et al. [47] detected absorption peak at 424 nm for silver nanoparticles derived from *Ceriops tagal*. The absorption peak we observed at 422 nm aligns well with these observations, mirroring findings by Rao and Paria [48], who studied nanoparticles from *Aegle marmelos* leaf extracts. In another study, the formation of AgNPs was

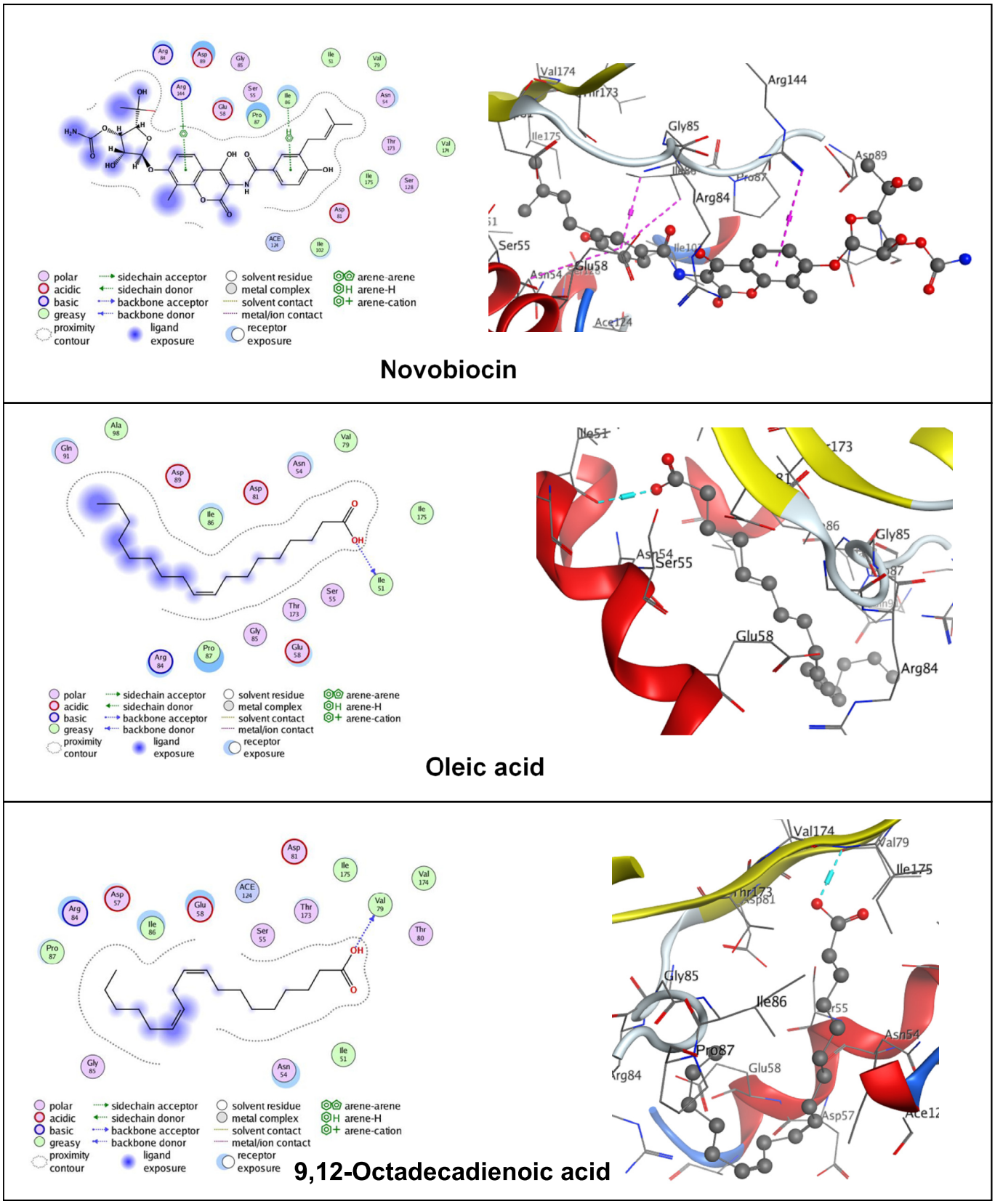

Fig. 7. Investigations using 2D and 3D molecular docking simulations of the interactions between the active site of the Gyrase B protein receptor (PDB ID: 4uro) and Novobiocin (Ligand) in the enzyme binding pocket, oleic acid, and 9,12-octadecadienoic acid.

validated by a color shift in *Chroococcus cyanobacterium* from pale yellow to deep brown, with a distinct peak at approximately 420 nm [49]. UV–visible spectroscopy of AgNPs made using *Padina pavonia* powder, according to Abdel-Raouf et al. [50], showed a

Table 4
Calculating docking interaction data between the active site of the GST protein receptor (PDB ID: **1PN9**) and the enzyme binding pocket of s-Hexylglutathione ligand (GTX), oleic acid, and 9,12-octadecadienoic acid.

Compound	Energy score (S) (Kcal/mol)	Affinity Bond strength (Kcal/mol)	Affinity Bond length (in A° from main residue)	Amino acids	Ligand	Interaction
s-Hexylglutathione ligand	−5.5076	−2	3.02	TYR 105	O 36	H-acceptor
Oleic acid	−5.9952	−1.5	2.93	GLU 202	O 53	H-donor
9,12-Octadecadienoic acid	−6.0975	−1.5	3	GLU 202	O 51	H-donor
		−4	2.8	GLY 8	O 50	H-acceptor

peak at 401 nm that grew stronger over time. The synthesis of AgNPs was carried out by Mishra et al. [51] using $AgNO_3$ in combination with *Chaetoceros* sp., *Skeletonema* sp., and *Thalassiosira* sp. They noticed a color shift over 48 h, going from colorless to pale yellow and finally reddish-brown, with peaks at 412 nm, 425 nm, and 430 nm, respectively, signifying the presence of biosynthesized AgNPs.

The color change marks the onset of nanoparticle formation, progressing from nucleation to growth where adjacent nucleonic particles combine to form thermodynamically stable AgNPs [51]. The interaction of radiation with metallic ions induces a transition to a higher energy state, producing an SPR band that reflects the nanoparticles' size and shape within a specific range [52]. According to Mie theory, size information derived from UV spectra shows that the SPR band for AgNP from *Chaetoceros* sp. occurs at a shorter wavelength of 412 nm, whereas for *Skeletonema* sp. and *Thalassiosira* sp., it shifts to longer wavelengths of 425 nm and 430 nm, respectively. These results are consistent with size estimates from DLS and SEM analysis [53].

Transmission electron microscopy remains a pivotal method for characterizing nanomaterials due to its ability to provide detailed insights into the morphology and size distribution of nanoparticles [54]. In this study, TEM was utilized to examine the structural and morphological details of silver nanoparticles synthesized from the marine algae *H. pannosa*. The TEM results clearly demonstrated the formation of AgNPs, corroborating findings from other studies that use marine macroalgae as eco-friendly sources for metal nanoparticle synthesis. These studies highlight the role of algal-derived phytochemicals in reducing metal ions to form nanoparticles [55]. Morphologically, the observed AgNPs were polydispersed in shape, including hexagons. This is significant as the shape of nanoparticles can substantially affect their properties and suitability for various applications. For example, spherical nanoparticles are often preferred for certain applications due to their enhanced biocompatibility and efficient cellular uptake [56]. The size distribution of the nanoparticles ranged from 15 to 60 nm, with two main groups: one between 15 and 40 nm and another between 40 and 60 nm, highlighting the polydispersity of the sample. This diversity in size, typical of biogenic synthesis, indicates the presence of nanoparticles of various dimensions within the sample [57]. TEM imaging also showed that AgNPs synthesized using *C. ellipsoidea* were quasi-spherical and varied in size [58], while those produced from P. *pavonia* powder were more uniform, primarily spherical and polygonal, ranging from 0.5 to 50 nm [50].

AgNPs made using *H. pannosa* showed a complex spectrum of peaks in the FT-IR analysis, indicating a complex composition of the algal extract. Similarly, in the alga *Dictyota mertensii*, a peak at 1383.8 cm^{-1} was linked to the silver reduction process [59]. As mentioned earlier, pectin, cellulose, and hemicellulose, which function as reducing and stabilizing agents, make up the majority of the cell walls of macro-sea alga [60]. These polymers' functional groups, in addition to proteinaceous materials and polysaccharides, are probably responsible for the reduction of silver salts to elemental silver (Ag^0). Because of their functional groups, these biological components help metal salts interact with them, which forms nanoparticles [61]. Moreover, the creation and stability of metal nanoparticles are significantly aided by uronic acids, polysaccharides, monosaccharides, and other biological compounds found in marine algae, such as secondary metabolites [62].

X-ray diffraction is a crucial technique for analyzing the structure of crystalline materials and is extensively used to investigate specific attributes such as crystal size, phase, quality, and other important characteristics of samples [63]. In this study, the XRD patterns showed peaks at angles of 27.27°, 31.98°, 38.03°, and 44.20°, corresponding to intensity values of 38.61, 21.36, 210.58, and 46.33, respectively. Similarly, Sahoo et al. [49] reported XRD patterns with peaks at 10.5°, 38.37°, and 64.4°, and corresponding intensity values of 86, 67, and 20. The presence of AgNPs was confirmed with peaks notably at 2-theta values of 38.37° and 64.4°; comparable XRD patterns at 38.2°, 44.3°, 64.6°, and 77.2° were recorded for the marine alga *Ecklonia cava* [64].

Furthermore, at 37.53°, 44.16°, 66.22°, and 76.74° corresponding to the crystallographic planes 111, 200, 220, and 311, respectively, four notable Bragg's reflections were noted. Using the Debye-Scherer equation, the average crystallite size of the produced AgNPs was found to be 17.7 nm [51]. These results align well with findings from other studies involving AgNPs synthesized from marine sources [65,66].

Zeta potential is a critical measure for assessing the stability of aqueous nanosuspensions, with a threshold of at least ±30 mV needed to consider the nanoparticles as a stable suspension [67]. In our research, the notably high negative zeta potential of −43.4 ± 10.6 mV significantly surpasses this threshold, indicating strong electrostatic repulsion among particles and affirming the stability of our biosynthesized AgNPs. This negative value, possibly influenced by the presence of nitrate ions, promotes repulsive forces across the particle surfaces, effectively preventing nanoparticle aggregation and ensuring stable dispersion resistant to spontaneous aggregation [67]. Furthermore, the PDI provides insight into the size variation of nanoparticles. A PDI of zero represents a monodisperse distribution, whereas a PDI of 1 indicates a high degree of polydispersity. Our results are in good agreement with those of Alzubaidi et al. [68], who found that silver nanoparticles made from an ethanolic flaxseed extract had a zeta potential of −44.5 mV. The average AgNP size was calculated using the DLS analysis to be 220.8 ± 31.3 nm, with a PDI of 0.408 [69]. On the other hand, the rEPS-SNPs showed a spherical shape with a mean diameter of 20.8 nm and sizes ranging from 8 to 36 nm. The average particle size, as shown by TEM micrographs, was 8.89 ± 6.95 nm. The discrepancy in size measurements between DLS and TEM might be attributed to solvent effects in DLS experiments, which can induce swelling of the nanoparticles [70]. Furthermore, 149.03 ± 3.04 nm, 186.73 ± 4.90 nm, and 239.46 ± 44.30 nm were the average particle sizes of AgNPs produced from *Chaetoceros* sp., *Skeletonema* sp., and *Thalassiosira* sp., respectively [51]. In the meantime, Sv/Ag-NPs obtained from *S. vulgare* showed a surface

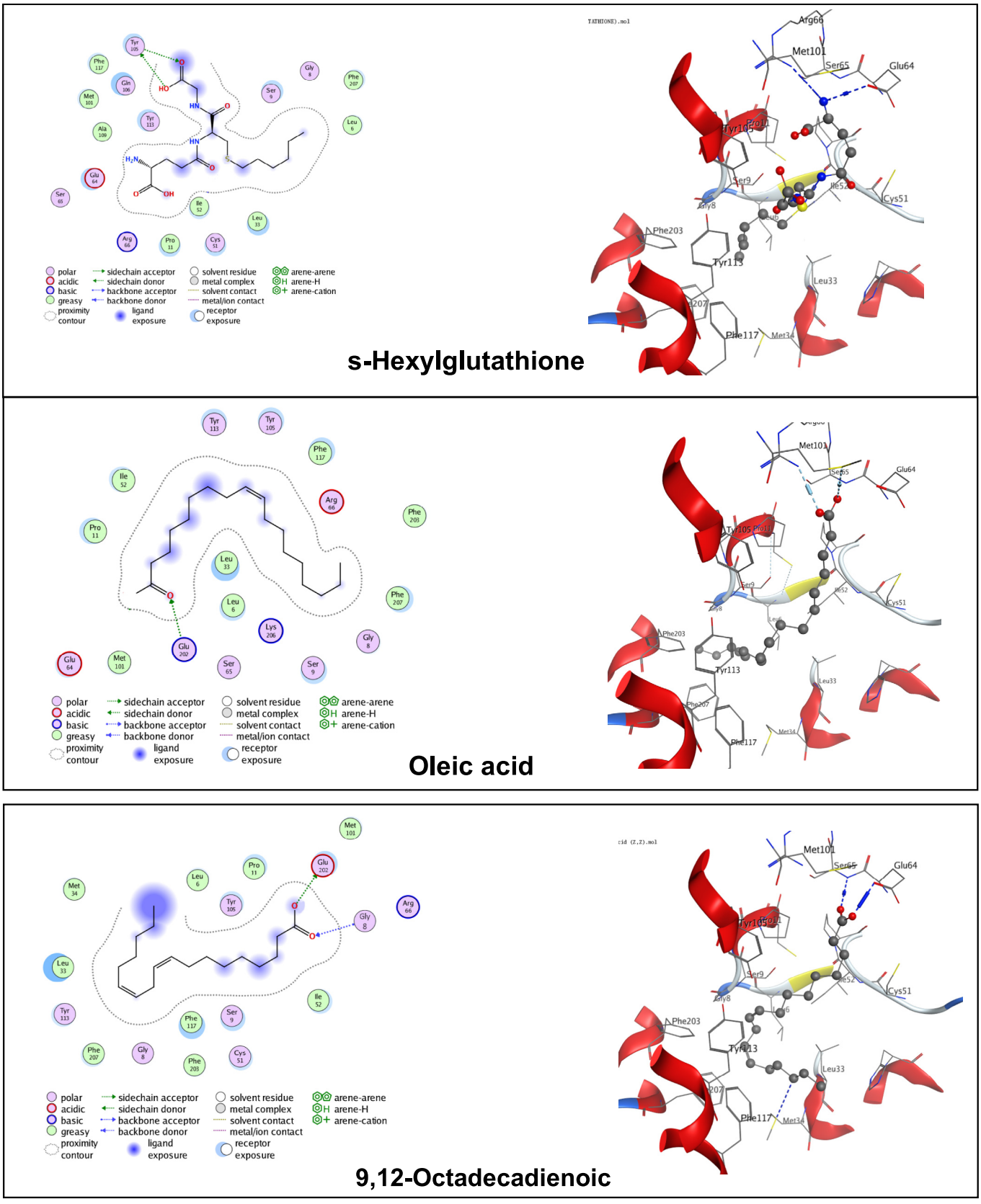

Fig. 8. Investigations using 2D and 3D molecular docking simulations of the interactions between the active site of the GST protein receptor (PDB ID: 1PN9) and the s-Hexylglutathione ligand (GTX) in the enzyme binding pocket, oleic acid, and 9,12-octadecadienoic acid.

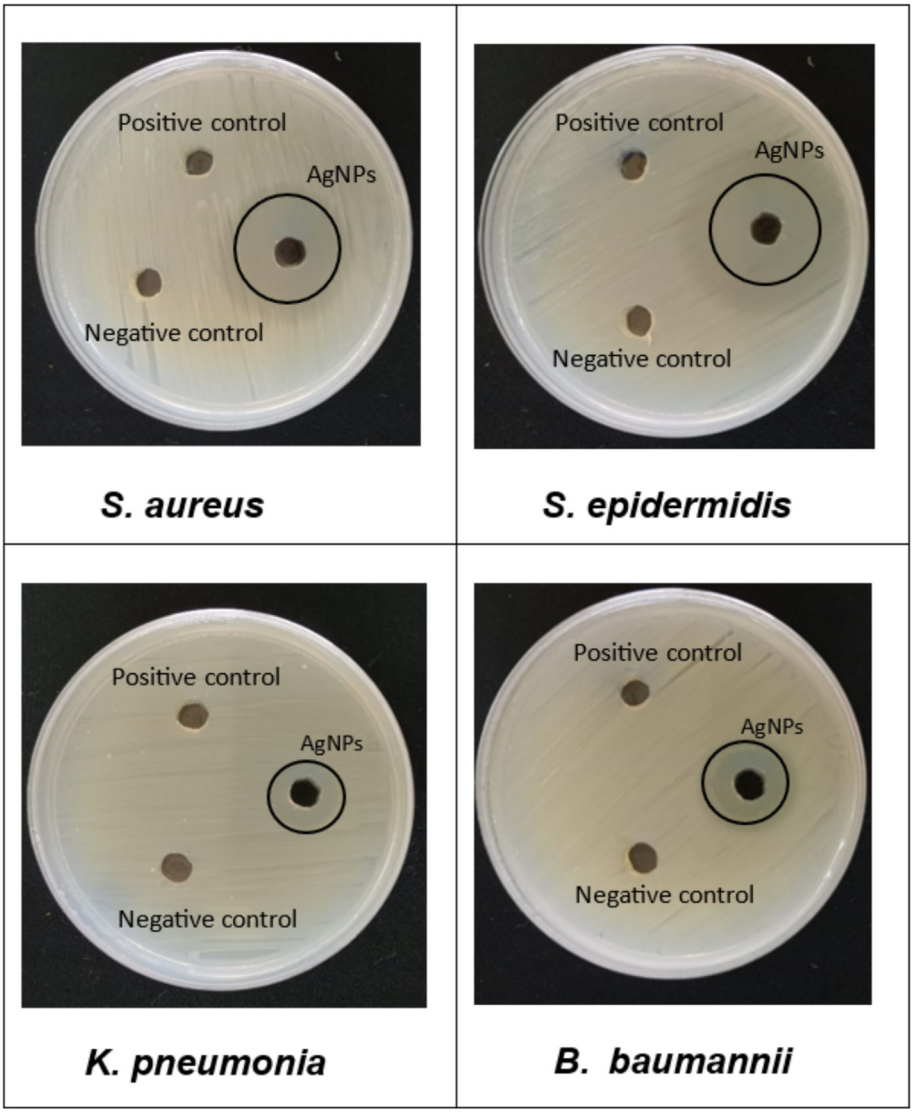

Fig. 9. Antibacterial activity of AgNPs by agar well approach.

Table 5
Antimicrobial activity of AgNPs biosynthesized by *H. pannosa*.

Microorganisms	Materials			
	Results of antimicrobial activity		Antibiotic	D. water
	R.	D. mm.	+ve control	–ve control
S. aureus	+ve	21	0	0
S. epidermidis	+ve	32	0	0
K. pneumonia	+ve	16	0	0
A. baumannii	+ve	21	0	0

Values represent the zone of inhibition (mm) against different microbial strains. "R" denotes resistance, and "D" indicates the diameter of inhibition.

Table 6
Minimum inhibitory concentrations and MBC of AgNPs.

No.	Isolate Name	MICs and MBCs by μg/mL.	
		MICs	MBCs
1	*S. aureus*	16	32
2	*S. epidermidis*	16	32
3	*K. pneumoniae*	32	32
4	*A. baumannii*	16	32

charge of –29.6 mV, as reported by Hamouda and Aljohani [71], indicating the common occurrence of negative zeta potentials in different silver nanoparticle syntheses.

10.2. GC/MS analysis

Red algae are prolific sources of various bioactive compounds, including phenolic compounds (such as phenols, phenolic acids, carotenoids, and flavonoids), as well as sterols and phytosterols,

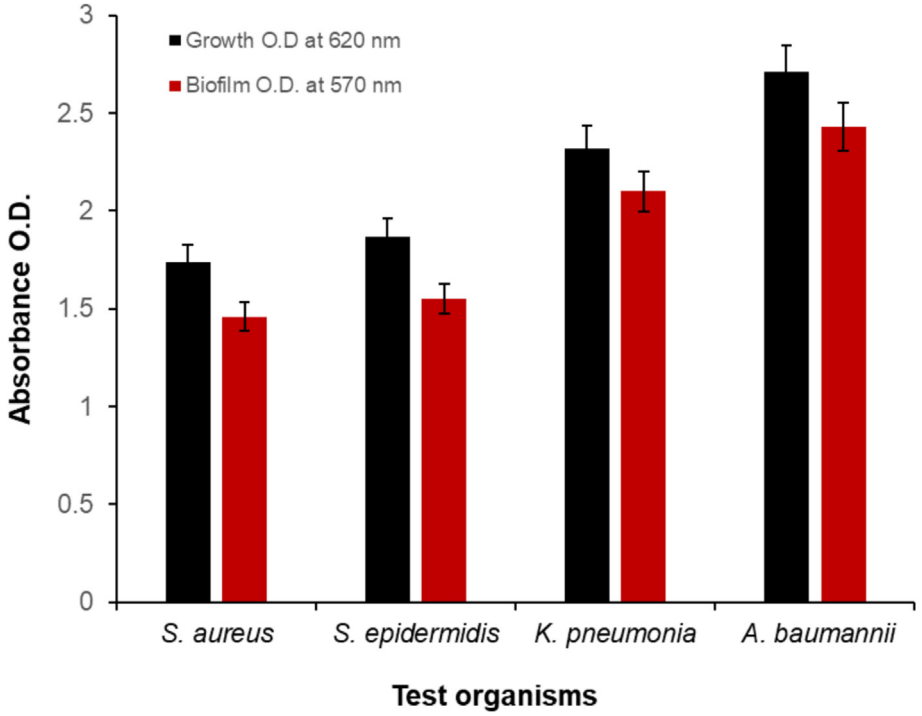

Fig. 10. Antibiofilm activity of AgNPs synthesized from *H. pannosa* against biofilm-forming bacteria.

Table 7
Larvicidal activity of algal and the synthesized AgNPs produced by *H. pannosa* extracts against *C. pipiens*, a mosquito vector.

Treatments	Concentrations (mg/L)	*n*	Larval mortality % ± SD	Regression equation	LC_{50} (LCL–UCL) (mg/L)	LC_{90} (LCL–UCL) (mg/L)	Statistic summary
Algal extract	Control	30	0.0 ± 0.0a	Y = 5.150X –13.100	349.786 (277.390– 422.315)	620.378 (493.692– 1117.762)	*d. f.* = 3, $P < 0.001$, $\chi^2 = 0.627$
	200	30	10.33 ± 9.50a				
	300	30	36.67 ± 5.77b				
	400	30	53.33 ± 5.77c				
	500	30	76.67 ± 5.77d				
	600	30	93.33 ± 5.77e				
AgNPs	Control	30	0.0 ± 0.0a	Y = 4.186X –6.867	43.674 (31.811– 55.293)	88.377 (67.473– 159.864)	*d. f.* = 3, $P < 0.001$, $\chi^2 = 1.653$
	20	30	13.33 ± 5.33b				
	40	30	36.67 ± 5.77c				
	60	30	63.33 ± 4.99d				
	80	30	86.67 ± 5.77e				
	100	30	100.0 ± 0.0f				
$AgNO_3$	Nil	Nil	Nil		Nil	Nil	Nil

The larval deaths are displayed as the mean ± SE of three duplicates. Significant differences exist between means with different letters ($p < 0.001$). The concentrations that kill 50% of the population at (LC50) and 90% of the population at (LC90), as well as the degrees of freedom (d. f.) and lower and upper confidence limits (UCL and LCL), Chi-square, n = sample size in (2).

which are precursors to vitamin A [72]. Benhniya et al. [73] conducted a GC/MS analysis of the dichloromethane/methanolic extract of *Pterosiphonia complanata* collected from the Sidi Bouzid site. The analysis identified various constituents, highlighting potential environmental impacts. Two major components were identified: n-hexadecanoic acid (palmitic acid) (15.68%) and neophytadiene (12.35%). Notably, most of the identified compounds exhibited antimicrobial activity. These results are in line with those of Mahmood Ansari et al. [74], who found that terpenes, alkaloids, amino acids, and fatty acids are among the many naturally occurring bioactive chemicals found in macromarine algae. These substances act as stabilizers and prevent the agglomeration of nanoparticles, underscoring the sea algae's multifunctionality in the creation and stabilization of nanoparticles.

10.3. Biological application

The antibacterial activity of AgNPs varies depending on the type of bacterial strains; when AgNPs were synthesized from red alga, they showed noteworthy efficacy against both Gram-positive and Gram-negative bacteria [75]. The largest zone of inhibition was 32 mm against *S. epidermidis*, followed by 21 mm against *S. aureus* and *A. baumannii*, and 16 mm against *K. pneumoniae*. The MIC for all tested organisms was consistently 16 μg/mL, except for *K. pneumoniae*, which had a MIC of 32 μg/mL. These results are corroborated by other studies [76,77]. With respect to *E. coli, S. aureus*, and *P. aeruginosa*, AgNPs demonstrated inhibition zones measuring 12–16 mm, and their corresponding MICs were 100 μg/mL, 200 μg/mL, and 100 μg/mL, respectively [49]. *S. typhimurium, S. faecalis*,

Table 8
The adulticidal properties of algal and the synthesized AgNPs derived from *H. pannosa* extracts were observed against the mosquito vector, *C. pipiens*.

Treatments	Concentrations (mg/L)	*n*	Adult mortality % ± SD	Regression equation	LC_{50} (LCL–UCL) (mg/L)	LC_{90} (LCL–UCL) (mg/L)	Statistic summary
Algal extract	Control	30	0.0 ± 0.0a	Y = 4.968X	299.810	543.004	*d. f.* = 3,
	200	30	23.33 ± 6.11a	−12.305	(222.636 – 362.119)	(434.994 – 948.917)	$P < 0.001$,
	300	30	46.67 ± 5.77b				$\chi^2 = 0.561$
	400	30	66.67 ± 5.77c				
	500	30	86.67 ± 4.98d				
	600	30	96.67 ± 5.77e				
AgNPs	Control	30	0.0 ± 0.0a	Y = 3.660X	45.595	102.121	*d. f.* = 3,
	20	30	16.67 ± 5.56b	−6.071	(32.345– 59.259)	(74.674– 219.447)	$P < 0.001$,
	40	30	33.33 ± 5.77c				$\chi^2 = 1.869$
	60	30	56.67 ± 6.02d				
	80	30	83.33 ± 5.77e				
	100	30	96.67 ± 5.09f				
$AgNO_3$	Nil	Nil	Nil		Nil	Nil	Nil

The larval deaths are displayed as the mean ± SE of three duplicates. Significant differences exist between means with different letters ($p < 0.001$). The concentrations that kill 50% of the population at (LC50) and 90% of the population at (LC90), as well as the degrees of freedom (d. f.) and lower and upper confidence limits (UCL and LCL), Chi-square, n = sample size in (2).

and *E. coli* were all inhibited by *Cymodocea turgidus* [78]. *Aeruginosa, E. coli*, and *S. aureus* had MICs of 43.94 μg/mL, 68.6 μg/mL, and 44.02 μg/mL for the AgNPs that were produced using *Gracilaria lanceolarium* leaf extract, respectively [79].

Furthermore, AgNPs produced by *Cyclotella calcitrans* demonstrated inhibition against multiple pathogens including *Klebsiella* spp., *Proteus vulgaris, P. aeruginosa*, and *E. coli* [80]. *Brevibacterium frigoritolerans*-derived AgNPs inhibited a range of bacteria including *Candida albicans* and *Vibrio parahaemolyticus* with zones ranging from 11 mm to 25 mm [81]. Fungus-mediated AgNPs displayed zones of inhibition against several bacteria including *E. coli* and *Salmonella enteritidis* with values between 6 mm and 10 mm [82]. The antibacterial mechanism of AgNPs is hypothesized to involve attachment to bacterial cell walls, causing structural changes through the formation of free radicals, as confirmed by electron spin resonance studies. The release of Ag^+ ions, which attach to negatively charged bacterial cell membranes, alongside the electrostatic forces, are crucial for the interaction of AgNPs with bacteria [83]. Additionally, the smaller size and greater surface area of nanoparticles enhance their microbial inhibitory activity by facilitating more direct interactions with pathogens [84]. Reactive oxygen species (ROS) creation, direct damage to cell membranes, and the absorption of free silver ions interfering with ATP synthesis and DNA replication are common mechanisms of nano-silver activity in bacteria [58].

The biofilm are crucial for bacterial survival in harsh environments, both within and outside a host, and contribute significantly to chronic and persistent infections [85]. The effectiveness of AgNPs in inhibiting biofilm formation was evaluated against four pathogenic organisms. The effectiveness values were as follows: *A. baumannii* at 2.710, *K. pneumoniae* at 2.320, *S. epidermidis* at 1.870, and *S. aureus* at 1.740. These values indicate the nanoparticles' relative efficacy in preventing biofilm formation, with higher values denoting stronger inhibition. Vázquez-Rodríguez et al. [70] observed a dose–response relationship in the antibiofilm activity of reduced EPS silver nanoparticles (rEPS-SNPs), which completely blocked biofilm development in *S. aureus*, achieving 100% inhibition. In another study, Kalishwaralal et al. [86] found that 50 mM of AgNPs, synthesized using *B. licheniformis* biomass, significantly inhibited biofilm formation in *P. aeruginosa* [49]. Arya et al. [87] also reported biofilm inhibition in *B. subtilis* and *P. aeruginosa* using biosynthesized AgNPs derived from *Prosopis juliflora* leaf extract. Further, AgNPs obtained from *S. anacardium* and *B. retusa*, at concentrations of 50 μg/ml and 60 μg/ml respectively, reduced biofilm formation by over 99%. The MICs needed for biofilm inhibition were found to be 68.94 ± 0.2 μg/mL, 12.9 ± 0.2 μg/ml, and 23.48 ± 0.2 μg/mL for AgNPs derived from *G. lanceolarium, S. anacardium*, and *B. retusa*, respectively [79]. Biofilm formation in bacteria primarily involves the synthesis and secretion of exopolysaccharides (EPSs), which are essential for the development of biofilms [88].

10.4. Larvicidal studies

One of the biggest issues facing public health in developing nations is mosquito-borne illnesses. Because of mosquito resistance, employing synthetic pesticides as a mosquitocidal repeatedly has become more difficult. Furthermore, toxicity to both people and non-target creatures all serve to heighten interest in investigating more environmentally friendly alternatives [89]. It has been thought that plant extracts make effective agent insecticides [90]. More and more data lately point to the possibility that green-fabricated mosquitocidal nanoparticles could be more successful than the plant extract under test [91]. There are little data on the toxicity of nanoparticles in relation to the *C. pipiens* filariasis vector [23,27,28,92,93].

Regarding the mode of action, we postulated that the toxicity of green-fabricated nanoparticles in mosquitoes might be caused by their small size, which enables them to enter individual cells and pass through the insect cuticle, interfering with biological processes such as molting. According to our findings, the larvicidal activity of algal and AgNPs produced by *H. pannosa* on *C. pipiens* mosquitoes demonstrated toxicity with LC50 and LC90 values of 349.786 and 620.378 mg/L, respectively, whereas the corresponding values for *H. pannosa*-mediated AgNPs were 43.674 and 88.377 mg/L. When compared to the control group, the concentrations of 600 and 100 mg/L of algal and AgNPs showed the highest larvicidal activity percentage (93.33 and 100), with no larval mortality seen in the group treated with $AgNO_3$ alone. The interaction between the silver in the nano range and the NH, C═O, COO^-, and C—N functional groups of proteins accounts for the good biological activity and adsorptive capacity of the AgNPs generated using algal extract [94]. According to recent research, cell lines, mosquitoes, and both Gram-positive and Gram-negative bacteria may be controlled by nanoparticles made from plant or marine sources [23,27,28,93]. Another study found that nanoparticles made with *Clausena dentate* were effective against *Aegypti, A. stephensi*, and *C. quinquefasciatus* mosquito species at concentrations of 240.714, 104.13, and 99.602 mg/L, respectively [95]. In contrast, *D. indica* was used to produce selenium nanoparticles, which were

more successful in suppressing early instar *A. aegypti* and *C. quinquefasciatus* at 0.39 and 1.11 mg/L, respectively, in the Krishnan et al. [96] investigation. When it comes to managing *A. aegypti* and *C. quinquefasciatus*, the toxicity of biologically produced AgNPs is just as good as that of selenium and gold nanoparticles, according to Zhang et al. [97]. Nonetheless, there are numerous additional relevant studies on naturally occurring extracts, such as the use of plant nanoparticles as insecticides. *Anopheles stephensi's* larvicidal activity was significantly increased by *Lagenaria siceraria* and its mediated ZnO-NPs, with an LC50 of 56.46 ppm [98]. When So-ZnO-NPs were tested against mosquitoes, their larvicidal activity was significantly stronger than that of the *S. officinalis* crude extract [23].

Our findings in the same study showed that AgNPs had the highest larvicidal activity compared to crude. For algal and AgNPs, the obtained LC50 and LC90 values were (299.810 and 543.004 mg/L) and (45.595 and 102.121 mg/L), respectively. While adult mortality reached the same concentration (96.67%) at 100 mg/L of AgNPs, it reached 96.67% at 600 mg/L of algal extract. Our research concurs with Soni and Prakash's [99] findings, which indicated that after 4 h of exposure, the adulticidal activity of *C. quinquefasciatus* was improved by AgNPs produced from *Azadirachta indica*, with an LC50 of 1.06 μL/cm^2. Similarly, *Feronia elephantum* reported by Hasaballah et al. [23] reported that the So-ZnO-NPs severely induced larvicidal activity for tested mosquitoes with LC50 and LC90 of 31.823 and 80.09 ppm for *C. pipiens* and 12.634 and 66.118 ppm for *Anopheles pharoensis*, respectively. According to Benelli [100], *Acacia caesia* leaf extract and manufactured AgNPs have a high adulticidal action against *An. subpictus* (LD50 = 18.66 μg/mL), *Ae. albopictus* (LD50 = 20.94 μg/mL), and *C. tritaeniorhynchus* (LD50 = 22.63 μg/mL). Our results are comparable to their findings. Furthermore, Suresh et al.'s [101] findings showed that adulticidal activity ended in the death of treated adults at LC50 and LC90 values of 174.14 and 422.29 for crude oil and 6.68 ppm and 23.58 ppm for *Phyllanthus niruri* AgNPs, respectively.

11. Conclusion

In this study, AgNPs were formed by reduction, capped, and stabilized using an extract from *H. pannosa*. Various analytical techniques, including UV–Vis spectroscopy, XRD, TEM, DLS, and FT-IR, confirmed the successful synthesis and characterization of the AgNPs. The surface plasmon resonance peak was observed at 420 nm, and structural analysis showed the nanoparticles to be crystalline, polydispersed, with an average size of 38 nm. The synthesized AgNPs demonstrated notable antimicrobial effects against Gram-positive and Gram-negative pathogens, with zones of inhibition indicating broad-spectrum potential. The MIC values were predominantly 16 μg/mL across tested organisms, except for *K. pneumoniae*, which required 32 μg/mL. The AgNPs also showed significant antibiofilm activity against four pathogenic strains, with inhibition values of 2.710 for *A. baumannii*, 2.320 for *K. pneumoniae*, 1.870 for *S. epidermidis*, and 1.740 for *S. aureus*. Furthermore, the AgNPs exhibited promising larvicidal and adulticidal effects against *Culex pipiens* mosquitoes, surpassing the efficacy of the extract of *H. pannosa* and underscoring their potential as eco-friendly agents for vector control.

CRediT authorship contribution statement

Mansour A.E. Bashar: Writing – original draft, Software, Formal analysis, Data curation, Conceptualization. **Enas M.H. Attia:** Software, Methodology, Investigation, Data curation. **Alsayed E. Mekky:** Visualization, Validation, Conceptualization. **Tharwat A. Selim:** Investigation, Formal analysis, Data curation, Conceptualization. **Walaa M. Shaban:** Formal analysis, Data curation, Conceptualization. **Mohamed A.M. El-Tabakh:** Writing – original draft, Resources, Methodology, Data curation. **Ammar.M. Mahmoud:** Formal analysis, Data curation, Conceptualization. **Mostafa A. Abdel-Maksoud:** Methodology, Investigation, Conceptualization. **Ali A. Ali:** Methodology, Investigation, Conceptualization. **Mohamed A. El-Tayeb:** Resources, Methodology, Data curation. **Waleed B. Suleiman:** Validation, Software, Data curation. **Mohamed E. El Beeh:** Software, Resources, Formal analysis, Conceptualization. **Sabiha Fatima:** Funding acquisition, Data curation. **Bushra Hafeez Kiani:** Investigation, Data curation, Conceptualization. **Nehal M. Khairy:** Validation, Software, Resources, Conceptualization. **Ebrahim Saied:** Writing – review & editing, Writing – original draft, Methodology, Formal analysis, Conceptualization.

Financial support

This work was funded by the Researchers Supporting Project number (RSPD2025R966), King Saud University, Riyadh, Saudi Arabia.

Declaration of competing interest

The authors declare that they have no conflict of interest.

Supplementary material

https://doi.org/10.1016/j.ejbt.2024.12.001.

Data availability

Data will be made available on request.

References

[1] Salam MA, Al-Amin MY, Salam MT, et al. Antimicrobial resistance: A growing serious threat for global public health. *Healthcare* 2023;11(13):1946. https://doi.org/10.3390/healthcare11131946. PMID: 37444780.
[2] Schulze A, Mitterer F, Pombo JP, et al. Biofilms by bacterial human pathogens: Clinical relevance-development, composition and regulation-therapeutical strategies. *Microbial Cell* 2021;8:28. https://doi.org/10.15698/mic2021.02.741. PMID: 33553418.
[3] Mahto KU, Priyadarshanee M, Samantaray DP, et al. Bacterial biofilm and extracellular polymeric substances in the treatment of environmental pollutants: Beyond the protective role in survivability. *J Clean Prod* 2022;379:134759. https://doi.org/10.1016/j.jclepro.2022.134759.
[4] Rather MA, Gupta K, Mandal M, et al. Microbial biofilm: Formation, architecture, antibiotic resistance, and control strategies. *Braz J Microbiol* 2021:1–18. https://doi.org/10.1007/s42770-021-00624-x. PMID: 34558029.
[5] Vincent F, Nueda A, Lee J, et al. Phenotypic drug discovery: Recent successes, lessons learned and new directions. *Nat Rev Drug Discov* 2022;21:899–914. https://doi.org/10.1038/s41573-022-00472-w. PMID: 35637317.
[6] Linklater DP, Ivanova EP. Nanostructured antibacterial surfaces–what can be achieved? *Nano Today* 2022;43:101404. https://doi.org/10.1016/j.nantod.2022.101404.
[7] Ahmed SF, Mofijur M, Rafa N, et al. Green approaches in synthesising nanomaterials for environmental nanobioremediation: Technological advancements, applications, benefits and challenges. *Environ Res* 2022;204:111967. https://doi.org/10.1016/j.envres.2021.111967. PMID: 34450159.
[8] Niculescu A-G, Chircov C, Bîrcă AC, et al. Nanomaterials synthesis through microfluidic methods: An updated overview. *Nanomaterials* 2021;11:864. https://doi.org/10.3390/nano11040864. PMID: 33800636.
[9] Kumar S, Jain S, Nehra M, et al. Green synthesis of metal–organic frameworks: A state-of-the-art review of potential environmental and medical applications. *Coord Chem Rev* 2020;420:213407. https://doi.org/10.1016/j.ccr.2020.213407.
[10] Ren Y, Sun H, Deng J, et al. Carotenoid production from microalgae: Biosynthesis, salinity responses and novel biotechnologies. *Mar Drugs* 2021;19:713. https://doi.org/10.3390/md19120713. PMID: 34940712.
[11] Rana A, Yadav K, Jagadevan S. A comprehensive review on green synthesis of nature-inspired metal nanoparticles: Mechanism, application and toxicity. *J Clean Prod* 2020;272:122880. https://doi.org/10.1016/j.jclepro.2020.122880.

[12] Aziz E, Batool R, Khan MU, et al. An overview on red algae bioactive compounds and their pharmaceutical applications. *J Complement Integr Med* 2021;17:20190203. https://doi.org/10.1515/jcim-2019-0203. PMID: 32697756.
[13] Malik SAA, Bedoux G, Maldonado JQG, et al. Defence on surface: Macroalgae and their surface-associated microbiome. *Adv Bot Res* 2020:327–68. https://doi.org/10.1016/bs.abr.2019.11.009.
[14] Qureshi A, Blaisi NI, Abbas AA, et al. Prospectus and development of microbes mediated synthesis of nanoparticles. *Microb Nanotechnol: Green Synth Appl* 2021:1–15. https://doi.org/10.1007/978-981-16-1923-6_1.
[15] Qari R, Haider S. Biochemical Analysis, Yield of Agar and its Physical and Chemical Characteristics of Marine Red Seaweeds of *Hypnea musciformis* (Wulfen) *JV Lamouroux*, *Hypnea pannosa J. Agardh*, *Hypnea valentiae* (Turner) Montagne from Karachi Coast. Microbiology 2020;3:34–44.
[16] Zarei Jeliani Z, Sohrabipour J, Soltani M, et al. Seasonal variations in growth and phytochemical compounds of cultivated red alga, *Hypnea flagelliformis*, in southern coastlines of Iran. *J Appl Phycol* 2021;33:2459–70. https://doi.org/10.1007/s10811-021-02429-9.
[17] Nqakala ZB, Sibuyi NRS, Fadaka AO, et al. Advances in nanotechnology towards development of silver nanoparticle-based wound-healing agents. *Int J Mol Sci* 2021;22:11272. https://doi.org/10.3390/ijms222011272. PMID: 34681930.
[18] Tufail MS, Liaqat IJP. Silver nanoparticles and their applications-a comprehensive review. *Pure Appl Biol* 2021;11:315–30. https://doi.org/10.19045/bspab.2022.110033.
[19] Bekele T, Alamnie GJAAC. Treatment of antibiotic-resistant bacteria by nanoparticles: Current approaches and prospects. *Ann Adv Chem* 2022;6:001–9. https://doi.org/10.29328/journal.aac.1001025.
[20] Mikhailova EO. Silver nanoparticles: Mechanism of action and probable bio-application. *J Funct Biomater* 2020;11:84. https://doi.org/10.3390/jfb11040084. PMID: 33255874.
[21] Chugh D, Viswamalya V, Das B, et al. Green synthesis of silver nanoparticles with algae and the importance of capping agents in the process. *J Genet Eng Biotechnol* 2021;19:126. https://doi.org/10.1186/s43141-021-00228-w. PMID: 34427807.
[22] Annamalai J, Ummalyma SB, Pandey A, et al. Recent trends in microbial nanoparticle synthesis and potential application in environmental technology: A comprehensive review. *Environ Sci Pollut Res* 2021;28:49362–82. https://doi.org/10.1007/s11356-021-15680-x. PMID: 34331227.
[23] Hasaballah AI, El-Naggar HA, Abdelbary S, et al. Eco-friendly synthesis of zinc oxide nanoparticles by marine sponge, *Spongia officinalis*: Antimicrobial and insecticidal activities against the mosquito vectors, *Culex pipiens* and *Anopheles pharoensis*. *BioNanoScience* 2022:1–16. https://doi.org/10.1007/s12668-021-00926-2.
[24] Mahmoud AM, El-Naggar HA, Hasaballah AI, et al. Aquatic insects as a biomonitoring and bioindicators for trace metals in the contaminated Al-Mahmoudia Canal, River Nile, Egypt. *Egypt J Aquat Biol Fish* 2022;26:365–86.
[25] Abdallah F, Rady M, Merdan B, et al. Effects of blood sources and artificial blood feeding membranes on the biological parameters and hepatitis c virus infectivity of *Culex pipiens* (diptera: Culicidae). *Afr Entomol* 2021;29:262–73., https://hdl.handle.net/10520/ejc-ento_v29_n1_a25.
[26] Ghosh A, Chowdhury N, Chandra G, et al. Plant extracts as potential mosquito larvicides. *Indian J Med Res* 2012;135:581–98. PMID: 22771587.
[27] Hashem AH, Selim TA, Alruhaili MH, et al. Unveiling antimicrobial and insecticidal activities of biosynthesized selenium nanoparticles using prickly pear peel waste. *J Funct Biomater* 2022;13:112. https://doi.org/10.3390/jfb13030112. PMID: 35997450.
[28] Selim TA, Abd-El Rahman IE, Mahran HA, et al. Mosquitocidal activity of the methanolic extract of *Annickia chlorantha* and its isolated compounds against *Culex pipiens*, and their impact on the non-target organism zebrafish, danio rerio. *Insects* 2022;13:676. https://doi.org/10.3390/insects13080676. PMID: 36005300.
[29] Prasad AR, Williams L, Garvasis J, et al. Applications of phytogenic zno nanoparticles: A review on recent advancements. *J Mol Liq* 2021;331:115805. https://doi.org/10.1016/j.molliq.2021.115805.
[30] Vieira AP, Stein EM, Andreguetti DX, et al. Preparation of silver nanoparticles using aqueous extracts of the red algae *laurencia aldingensis* and *laurenciella* sp. and their cytotoxic activities. *J Appl Phycol* 2016;28:2615–22. https://doi.org/10.1007/s10811-015-0757-4.
[31] Albalawi MA, Abdelaziz AM, Attia MS, et al. Mycosynthesis of silica nanoparticles using *Aspergillus niger*: Control of *Alternaria solani* causing early blight disease, induction of innate immunity and reducing of oxidative stress in eggplant. *Antioxidants* 2022;11:2323. https://doi.org/10.3390/antiox11122323. PMID: 36552531.
[32] Hajam YA, Rai S, Kumar R, et al. Phenolic compounds from medicinal herbs: Their role in animal health and diseases–a new approach for sustainable welfare and development. *Plant Phenolics Sustain Agric* 2020:221–39. https://doi.org/10.1007/978-981-15-4890-1_10.
[33] Farkas N, Kramar JA. Dynamic light scattering distributions by any means. *J Nanopart Res* 2021;23:120. https://doi.org/10.1007/s11051-021-05220-6. PMID: 39381776.
[34] Devi L, Gupta R, Jain SK, et al. Synthesis, characterization and in vitro assessment of colloidal gold nanoparticles of gemcitabine with natural polysaccharides for treatment of breast cancer. *J Drug Delivery Sci Technol* 2020;56:101565. https://doi.org/10.1016/j.jddst.2020.101565.
[35] de Santi II, Pacheco BS, Venzke D, et al. Sterols in red macroalgae from Antarctica: Extraction and quantification by gas chromatography–mass spectrometry. *Polar Biol* 2021;44:987–95. https://doi.org/10.1007/s00300-021-02853-0.
[36] Jama MA, Mohammed OH, Guled AA, et al. Isolation and identification of pathogenic bacteria in pond water and fish body and evaluation of their antibiotic susceptibility. *J Fish Aquac Res* 2020;5:054–60.
[37] Sharmila G, Muthukumaran C, Sangeetha E, et al. Green fabrication, characterization of *Pisonia alba* leaf extract derived MgO nanoparticles and its biological applications. *Nano-Struct Nano-Objects* 2019;20:100380. https://doi.org/10.1016/j.nanoso.2019.100380.
[38] Bakht Dalir SJ, Djahaniani H, Nabati F, et al. Characterization and the evaluation of antimicrobial activities of silver nanoparticles biosynthesized from *Carya illinoinensis* leaf extract. *Heliyon* 2020;6. https://doi.org/10.1016/j.heliyon.2020.e03624. PMID: 32215333.
[39] Faisal S, Shah SA, Shah S, et al. In vitro biomedical and photo-catalytic application of bio-inspired Zingiber officinale mediated silver nanoparticles. *J Biomed Nanotechnol* 2020;16:492–504. https://doi.org/10.1166/jbn.2020.2918. PMID: 32970981.
[40] Mekky AE, Farrag AA, Hmed AA, et al. Antibacterial and antifungal activity of green-synthesized silver nanoparticles using *Spinacia oleracea* leaves extract. *Egypt J Chem* 2021;64:5781–92. https://doi.org/10.21608/ejchem.2021.74432.3673.
[41] CRyPTIC Consortium. Epidemiological cut-off values for a 96-well broth microdilution plate for high-throughput research antibiotic susceptibility testing of M. tuberculosis. Eur Respir J 2022;60(4). https://doi.org/10.1183/13993003.00239-2022. PMID: 35301246.
[42] Luna B, Trebosc V, Lee B, et al. A nutrient-limited screen unmasks rifabutin hyperactivity for extensively drug-resistant acinetobacter baumannii. *Nat Microbiol* 2020;5:1134–43. https://doi.org/10.1038/s41564-020-0737-6. PMID: 32514072.
[43] Mekky AE, Abdelaziz AE, Youssef FS, et al. Unravelling the antimicrobial, antibiofilm, suppressing fibronectin binding protein A (fnba) and cna virulence genes, anti-inflammatory and antioxidant potential of biosynthesized *Solanum lycopersicum* silver nanoparticles. *Medicina* 2024;60:515. https://doi.org/10.3390/medicina60030515. PMID: 38541241.
[44] Larvicides MO. Guidelines for laboratory and field testing of mosquito larvicides. Google Scholar 2005.
[45] Finney DJ. Probit analysis. Cambridge, UK: Cambridge University Press; 1971.
[46] Abdel-Raouf N, Al-Enazi NM, Ibraheem IB, et al. Green biosynthesis of gold nanoparticles using *Galaxaura elongata* and characterization of their antibacterial activity. *Arab J Chem* 2017;10:S3029–39. https://doi.org/10.1016/j.arabjc.2013.11.044.
[47] Dhas SP, Mukerjhee A, Chandrasekaran N, et al. Phytosynthesis of silver nanoparticles using *Ceriops tagal* and its antimicrobial potential against human pathogens. *Int J Pharm Pharm Sci* 2013;5:349–52.
[48] Rao KJ, Paria S. Green synthesis of silver nanoparticles from aqueous *Aegle marmelos* leaf extract. *Mater Res Bull* 2013;48:628–34. https://doi.org/10.1016/j.materresbull.2012.11.035.
[49] Sahoo CR, Maharana S, Mandhata CP, et al. Biogenic silver nanoparticle synthesis with cyanobacterium *Chroococcus minutus* isolated from Baliharachandi sea-mouth, Odisha, and in vitro antibacterial activity. *Saudi J Biol Sci* 2020;27(6):1580–6. https://doi.org/10.1016/j.sjbs.2020.03.020. PMID: 32489298.
[50] Abdel-Raouf N, Al-Enazi NM, Ibraheem IB, et al. Biosynthesis of silver nanoparticles by using of the marine brown alga *Padina pavonia* and their characterization. *Saudi J Biol Sci* 2019;26(6):1207–15. https://doi.org/10.1016/j.sjbs.2018.01.007. PMID: 31516350.
[51] Mishra B, Saxena A, Tiwari AJBR, et al. Biosynthesis of silver nanoparticles from marine *diatoms chaetoceros* sp., *skeletonema* sp., *thalassiosira* sp., and their antibacterial study. *Biotechnol Rep* 2020;28:e00571. https://doi.org/10.1016/j.btre.2020.e00571. PMID: 33312881.
[52] Tang H, Chen CJ, Huang Z, et al. Plasmonic hot electrons for sensing, photodetection, and solar energy applications: A perspective. J Chem Phys 2020;152(22). https://doi.org/10.1063/5.0005334. PMID: 32534522.
[53] Duque JS, Blandón JS, Riascos H. Localized Plasmon resonance in metal nanoparticles using Mie theory. *J Phys Conf Ser* 2017;850(1):012017. https://doi.org/10.1088/1742-6596/850/1/012017.
[54] Srivastava S, Bhargava A. Green nanoparticles: the future of nanobiotechnology. Singapore: Springer; 2022.
[55] Chopra H, Bibi S, Singh I, et al. Green metallic nanoparticles: Biosynthesis to applications. Front Bioeng Biotechnol 2022;10:874742. https://doi.org/10.3389/fbioe.2022.874742. PMID: 35464722.
[56] Salata OV. Applications of nanoparticles in biology and medicine. J Nanobiotechnol 2004;2:1–6. https://doi.org/10.1186/1477-3155-2-3. PMID: 15119954.
[57] Kuppusamy P, Yusoff MM, Maniam GP, et al. Biosynthesis of metallic nanoparticles using plant derivatives and their new avenues in pharmacological applications–an updated report. *Saudi Pharm J* 2016;24:473–84. https://doi.org/10.1016/j.jsps.2014.11.013. PMID: 27330378.
[58] Ibraheem IB, Abd-Elaziz BE, Saad WF, et al. Green biosynthesis of silver nanoparticles using marine Red Algae *Acanthophora specifera* and its antimicrobial activity. *J Nanomedi Nanotechnol* 2016;7(409):1–4. https://doi.org/10.4172/2157-7439.1000409.

[59] Fernandes-Negreiros MM, Araujo Machado RI, Bezerra FL, et al. Antibacterial, antiproliferative, and immunomodulatory activity of silver nanoparticles synthesized with fucans from the alga *Dictyota mertensii*. *Nanomaterials* 2017;8(1):6. https://doi.org/10.3390/nano8010006. PMID: 29295570.
[60] Zaki M, Abdul Khalil HPS, Sabaruddin F, et al. Microbial treatment for nanocellulose extraction from marine algae and its applications as sustainable functional material. *Bioresour Technol Rep* 2021;16:100811. https://doi.org/10.1016/j.biteb.2021.100811.
[61] Gahlawat G, Choudhury AR. A review on the biosynthesis of metal and metal salt nanoparticles by microbes. *RSC Adv* 2019;9:12944–67. https://doi.org/10.1039/c8ra10483b. PMID: 35520790.
[62] Jönsson M, Allahgholi L, Sardari RR, et al. Extraction and modification of macroalgal polysaccharides for current and next-generation applications. *Molecules* 2020;25:930. https://doi.org/10.3390/molecules25040930. PMID: 32093097.
[63] Fatima R, Priya M, Indurthi L, et al. Biosynthesis of silver nanoparticles using red algae *Portieria hornemannii* and its antibacterial activity against fish pathogens. *Microb Pathog* 2020;138:103780. https://doi.org/10.1016/j.micpath.2019.103780. PMID: 31622663.
[64] Venkatesan J, Kim S-K, Shim MSJN, et al. Antimicrobial, antioxidant, and anticancer activities of biosynthesized silver nanoparticles using marine algae *Ecklonia cava*. *Nanomaterials* 2016;6:235. https://doi.org/10.3390/nano6120235. PMID: 28335363.
[65] Mahyoub JA. Bioactivity of two marine algae extracts and their synthesized silver nanoparticles as safe controls against Musca domestica housefly. *Entomol Res* 2021;51(7):323–30. https://doi.org/10.1111/1748-5967.12512.
[66] Mahyoub JA, Aziz AT, Panneerselvam C, et al. Seagrasses as sources of mosquito nano-larvicides? Toxicity and uptake of Halodule uninervis-biofabricated silver nanoparticles in dengue and Zika virus vector *Aedes aegypti*. *J Clust Sci* 2017;28:565–80. https://doi.org/10.1007/s10876-016-1127-3.
[67] McNeil SE, editor. Characterization of nanoparticles intended for drug delivery. New York, NY: Humana press; 2011. https://doi.org/10.1007/978-1-4939-7352-1.
[68] Alzubaidi AK, Al-Kaabi WJ, Ali AA, et al. Green synthesis and characterization of silver nanoparticles using flaxseed extract and evaluation of their antibacterial and antioxidant activities. *Appl Sci* 2023;13(4):2182. https://doi.org/10.3390/app13042182.
[69] Borah D, Das N, Das N, et al. Alga-mediated facile green synthesis of silver nanoparticles: Photophysical, catalytic and antibacterial activity. Appl Organomet Chem 2020;34(5):e5597.
[70] Vázquez-Rodríguez A, Vasto-Anzaldo XG, Leon-Buitimea A, et al. Antibacterial and antibiofilm activity of biosynthesized silver nanoparticles coated with exopolysaccharides obtained from *Rhodotorula mucilaginosa*. IEEE Trans NanoBiosci 2020;19(3):498–503. https://doi.org/10.1109/TNB.2020.2985101. PMID: 32248119.
[71] Hamouda RA, Aljohani ES. Assessment of silver nanoparticles derived from brown algae *Sargassum vulgare*: Insight into antioxidants, anticancer, antibacterial and hepatoprotective effect. *Mar Drugs* 2024;22:154. https://doi.org/10.3390/md22040154. PMID: 38667771.
[72] Olfat A, Mostaghim T, Shahriari S, et al. Extraction of bioactive compounds of *Hypnea flagelliformis* by ultrasound-assisted extraction coupled with natural deep eutectic solvent and enzyme inhibitory activity. *Algal Res* 2024;78:103388. https://doi.org/10.1016/j.algal.2023.103388.
[73] Benhniya B, Lakhdar F, Rezzoum N, Etahiri S. GC/MS analysis and antibacterial potential of macroalgae extracts harvested on Moroccan Atlantic coast. Egypt J Chem 2022;65(132):171–9. https://doi.org/10.21608/ejchem.2022.117053.5301.
[74] Mahmood Ansari S, Saquib Q, De Matteis V, et al. Marine macroalgae display bioreductant efficacy for fabricating metallic nanoparticles: Intra/extracellular mechanism and potential biomedical applications. *Bioinorg Chem Appl* 2021;2021(1):5985377. https://doi.org/10.1155/2021/5985377. PMID: 34873399.
[75] Algotiml R, Gab-Alla A, Seoudi R, et al. Anticancer and antimicrobial activity of biosynthesized Red Sea marine algal silver nanoparticles. *Sci Rep* 2022;12(1):2421. https://doi.org/10.1038/s41598-022-06412-3. PMID: 35165346.
[76] Garibo D, Borbón-Nuñez HA, de León JN, et al. Green synthesis of silver nanoparticles using *Lysiloma acapulcensis* exhibit high-antimicrobial activity. *Sci Rep* 2020;10(1):12805. https://doi.org/10.1038/s41598-020-69606-7. PMID: 32732959.
[77] Liaqat N, Jahan N, Anwar T, et al. Green synthesized silver nanoparticles: Optimization, characterization, antimicrobial activity, and cytotoxicity study by hemolysis assay. *Front Chem* 2022;10:952006. https://doi.org/10.3389/fchem.2022.952006. PMID: 36105303.
[78] Hafez EE, Kabeil SS. Antimicrobial activity of nano-silver particles produced by micro algae. *J Pure Appl Microbio* 2013;1(7):35–42. , https://www.researchgate.net/publication/286395781.
[79] Mohanta YK, Biswas K, Jena SK, et al. Anti-biofilm and antibacterial activities of silver nanoparticles synthesized by the reducing activity of phytoconstituents present in the indian medicinal plants. *Front Microbiol* 2020;11:1143. https://doi.org/10.3389/fmicb.2020.01143. PMID: 32655511.
[80] Merin DD, Prakash S, Bhimba BV. Antibacterial screening of silver nanoparticles synthesized by marine micro algae. *Asian Pac J Trop Med* 2010;3:797–9. https://doi.org/10.1016/S1995-7645(10)60191-5.
[81] Singh SP, Bhargava CS, Dubey V, et al. Silver nanoparticles: Biomedical applications, toxicity, and safety issues. *Int J Res Pharm Pharm Sci* 2017;4(2):1. , https://www.researchgate.net/publication/330875019.
[82] Gond SK, Mishra A, Verma SK, et al. Synthesis and characterization of antimicrobial silver nanoparticles by an endophytic fungus isolated from Nyctanthes arbor-tristis. *Proc Natl Acade Sci, India Sect B: Biol Sci* 2020;90:641–5. https://doi.org/10.1007/s40011-019-01137-2.
[83] Tripathi N, Goshisht MK. Recent advances and mechanistic insights into antibacterial activity, antibiofilm activity, and cytotoxicity of silver nanoparticles. *ACS Appl Bio Mater* 2022;5:1391–463. https://doi.org/10.1021/acsabm.2c00014. PMID: 35358388.
[84] Nisar P, Ali N, Rahman L, et al. Antimicrobial activities of biologically synthesized metal nanoparticles: An insight into the mechanism of action. *J Biol Inorg Chem* 2019;24:929–41. https://doi.org/10.1007/s00775-019-01717-7. PMID: 31515623.
[85] Singh A, Amod A, Pandey P, et al. Bacterial biofilm infections, their resistance to antibiotics therapy and current treatment strategies. *Biomed Mater* 2022;17:022003. https://doi.org/10.1088/1748-605X/ac50f6. PMID: 35105823.
[86] Kalishwaralal K, BarathManiKanth S, Pandian SR, et al. Silver nanoparticles impede the biofilm formation by *Pseudomonas aeruginosa* and *Staphylococcus epidermidis*. *Colloids Surf B Biointerfaces* 2010;79:340–4. https://doi.org/10.1016/j.colsurfb.2010.04.014. PMID: 20493674.
[87] Arya G, Kumari RM, Gupta N, et al. Green synthesis of silver nanoparticles using *Prosopis juliflora* bark extract: Reaction optimization, antimicrobial and catalytic activities. *Artif Cells Nanomed Biotechnol* 2018;46:985–93. https://doi.org/10.1080/21691401.2017.1354302. PMID: 28720002.
[88] Gupta P, Pruthi PA, Pruthi V. Role of exopolysaccharides in biofilm formation. Introduction to biofilm engineering. *Am Chem Soc* 2019:17–57. https://doi.org/10.1021/bk-2019-1323.ch002.
[89] Benelli G. Mode of action of nanoparticles against insects. *Environ Sci Pollut Res* 2018;25:12329–41. https://doi.org/10.1007/s11356-018-1850-4. PMID: 29611126.
[90] Pavela R. Larvicidal effects of various euro-asiatic plants against *Culex quinquefasciatus* say larvae (diptera: Culicidae). *Parasitol Res* 2008;102:555–9. https://doi.org/10.1007/s00436-007-0821-3. PMID: 18058128.
[91] Murugan K, Panneerselvam C, Subramaniam J, et al. Eco-friendly drugs from the marine environment: Spongeweed-synthesized silver nanoparticles are highly effective on *Plasmodium falciparum* and its vector *Anopheles stephensi*, with little non-target effects on predatory copepods. *Environ Sci Pollut Res* 2016;23:16671–85. https://doi.org/10.1007/s11356-016-6832-9. PMID: 27180838.
[92] Murugan K, Anitha J, Suresh U, et al. Chitosan-fabricated ag nanoparticles and *larvivorous fishes*: A novel route to control the coastal malaria vector *Anopheles sundaicus*? *Hydrobiologia* 2017;797:335–50. https://doi.org/10.1007/s10750-017-3196-1.
[93] Hasaballah AI, Selim TA, Tanani MA, et al. Lethality and vitality efficiency of different extracts of Salix safsaf leaves against the house fly, *Musca domestica* L.(Diptera: Muscidae). Afr Entomol 2021;29(2):479–90. , https://hdl.handle.net/10520/ejc-ento_v29_n2_a17.
[94] Sowndarya P, Ramkumar G, Shivakumar MS. Green synthesis of selenium nanoparticles conjugated *Clausena dentata* plant leaf extract and their insecticidal potential against mosquito vectors. *Artif Cells Nanomed Biotechnol* 2017;45:1490–5. https://doi.org/10.1080/21691401.2016.1252383. PMID: 27832715.
[95] Rauf MA, Jolly J, Ahmad Z. Synthesis and characterization of nano-selenium using plant biomolecules and their potential applications. *Selenium and nano-selenium in environmental stress management and crop quality improvement*. Springer; 2022:25–40. https://doi.org/10.1007/978-3-031-07063-1_2.
[96] Krishnan M, Ranganathan K, Maadhu P, et al. Leaf extract of *Dillenia indica* as a source of selenium nanoparticles with larvicidal and antimicrobial potential toward vector mosquitoes and pathogenic microbes. *Coatings* 2020;10:626. https://doi.org/10.3390/coatings10070626.
[97] Zhang J, Wang H, Bao Y, et al. Nano red elemental selenium has no size effect in the induction of seleno-enzymes in both cultured cells and mice. *Life Sci* 2004;75(2):237–44. https://doi.org/10.1016/j.lfs.2004.02.004. PMID: 15120575.
[98] Kalpana VN, Alarjani KM, Rajeswari VD. Enhancing malaria control using *Lagenaria siceraria* and its mediated zinc oxide nanoparticles against the vector Anopheles stephensi and its parasite *Plasmodium falciparum*. *Sci Rep* 2020;10(1):21568. https://doi.org/10.1038/s41598-020-77854-w. PMID: 33298984.
[99] Soni N, Prakash S. Green nanoparticles for mosquito control. *Sci World J* 2014;2014(1):496362. https://doi.org/10.1155/2014/496362. PMID: 25243210.
[100] Benelli G. Plant-mediated synthesis of nanoparticles: A newer and safer tool against mosquito-borne diseases? *Asian Pac J Trop Biomed* 2016;6:353–4. https://doi.org/10.1016/j.apjtb.2015.10.015.
[101] Suresh U, Murugan K, Benelli G, et al. Tackling the growing threat of dengue: Phyllanthus niruri-mediated synthesis of silver nanoparticles and their mosquitocidal properties against the dengue vector *aedes aegypti* (diptera: Culicidae). *Parasitol Res* 2015;114:1551–62. https://doi.org/10.1007/s00436-015-4339-9. PMID: 25669140.